



Hochschule für Angewandte
Wissenschaften Hamburg
Hamburg University of Applied Sciences

Department Biomedical Engineering

Bachelor Thesis

Validation of Functional Calibration Methods for Inertial Motion Capture Units in Disturbed Magnetic Fields

submitted by Jakob Foehres

Enrolment number: XXXXXXXXXX

1. Reviewer:
Prof. Nicholas Bishop
2. Reviewer:
Dr. Peter Konrad

In Cooperation with:
Noraxon Inc
& Velamed GmbH

July 2020

Statutory Declaration

I, Jakob Foehres, student of the University of Applied Sciences in Hamburg, enrolment number 2270627, hereby affirm in lieu of oath, that I have have written this thesis independently, without the help of third parties or contributions other than those specified. The data, tables and graphics directly or indirectly taken over from other sources are marked under indication of the source. No one has directly or indirectly received monetary services from me, for work that is connected with the content of the submitted thesis. The paper was not previously presented to another examination board and has not been published.

Contents

Abstract	II
List of Figures	III
List of Tables	IV
1 Introduction	1
1.1 Problem Definition	1
1.2 Current Solutions	1
1.3 Proposed Solution	2
1.4 Hypothesis	2
2 Fundamentals	3
2.1 Planes of Human Motion	3
2.2 Anatomical terms of movement	4
2.3 IMU Technology	4
2.3.1 Sensor types	4
2.3.2 Earth Frame and Progression Frame	6
2.3.3 Sensor Fusion	8
2.4 Posture Calibration of IMU based models	8
2.5 Magnetic Field and Field Inhomogeneity	9
2.6 Functional Calibration Methods	10
2.6.1 Walking Calibration	11
2.6.2 Multipose	12
3 Materials and Methods	14
3.1 Test Procedure	14
3.2 Subject and Material	15
3.2.1 IMU System	15
3.2.2 Reference System	16
3.3 Calibration Spots	17
3.4 Data Acquisition	19
3.5 Data Analysis	20

3.6	Statistical Analysis	20
4	Results	22
4.1	Dirty Spot Calibration	22
4.1.1	Gait	22
4.1.2	Squats	27
4.2	Clean Spot Calibration	32
4.2.1	Squats	32
5	Discussion	37
5.1	General Annotations	37
5.2	Dirty Spot Calibration	39
5.3	Clean Spot Calibration	41
5.4	Summary	41
5.5	Limitations and suggestions for future research	43
6	Conclusion	45
	References	46
A	Gait Plots	i
B	Squat Plots	v
B.1	Dirty Spot Calibration	v
B.2	Clean Spot Calibration	xi
C	Offset tables	xviii

Abstract

In the field of biomechanics, Inertial Measurement Units play an increasingly important role in the kinematic analysis of human movement. The sensors are often instrumented with magnetometers, which give information about the alignment in an external reference frame. Since many users cannot guarantee magnetically homogeneous conditions in their facilities, the use of inertial motion capture technology is hereby limited. Researches and engineers face the challenge of developing easy-to-use calibration methods, which rely on the information of gyroscopes and accelerometers, to overcome this restriction.

In this study, two of those calibration methods are described. The procedures, developed by Noraxon Inc, follow different functional, two step approaches. The methods were validated against an optical reference system for movements of the lower limbs in gait and squat. Different data sets with initial pose calibrations in an assumed magnetically homogeneous and in an assumed magnetically inhomogeneous spot were evaluated.

Both examined Functional Calibration Methods show promising results for movements in sagittal and coronal plane. The methods correct heavily spoiled data in the inhomogeneous spot and increase Range of Motion and Root Mean Square Errors (RMSE) relative to the optical reference. The RMSE of sagittal movements stayed below 3° for all angles. Movements in the coronal plane show the highest errors for the original data in the disturbed magnetic spot and can be reduced to moderate RMSE below 5° . Qualitative analyzes of gait cycles confirm the findings. The results demonstrate the increased usability of the system, since they are comparable to common protocols for gait analysis. In the transversal plane, IMU data shows higher deviations to the reference up to RMSE of 7.96° . The deviations to the reference were high for both calibration spots, which shows the limitations of IMU technology for movements in this plane. The proposed Functional Calibration methods do not fundamentally increase nor deteriorate the quality of the signal in this plane.

Further investigation should focus on analysis of movements in the transversal plane and the offset between the IMU data of different calibration methods.

List of Figures

1	Planes of Human Motion	3
1a	Conventions for global reference frame and segmental local center of mass reference frame (Wu and Cavanagh 1995) . . .	3
1b	Human Planes	3
2	Anatomical Terms of Movement, adapted from (TeachMeAnatomy 2015)	4
3	Inertial Measurement Units	5
3a	Translatory and Rotatory Degrees of freedom	5
3b	MyoMotion Research Pro IMU, Two Sensors and Receiver . .	5
4	Attitude of the sensor in the earth frame (Cockroft 2015)	7
5	Alignment of the sensors with the lower limbs (Palermo et al. 2014) .	9
6	Qualitative Mapping with 15 identical compasses (De Vries et al. 2008)	10
7	Walking Calibration Procedure	11
8	Steps of Multipose Calibration (a)-(e)	12
8a	12
8b	12
8c	12
8d	12
8e	12
9	Measurement setup	15
10	Subject with attached sensors and CAST marker set	16
11	Position and labels of markers for the CAST marker set	17
12	Calibration spots with magnetometer table	18
12a	inhomogeneous spot in front of ergometer	18
12b	clean spot on plastic stool	18
13	Definition and explanation of a boxplot, from Galarnyk 2018	21
14	Gait curves, sagittal plane	22
14a	Left Ankle Dorsiflexion	22
14b	Right Knee Flexion	22
15	Gait curves, right knee and right hip abduction	24
16	Gait curves, ankle inversion	25

17	Gait curves, right and left ankle abduction	26
18	Gait curves, left hip and knee rotation	26
19	Dirty spot dorsiflexion error, left ankle	28
20	Dirty spot abduction error, right knee	29
21	Dirty spot abduction error, right hip	29
22	Dirty spot rotation error, left ankle	30
23	Dirty spot rotation error, left knee	31
24	Dirty spot abduction error, left ankle	31
25	Clean spot dorsiflexion error, right ankle	33
26	Clean spot abduction error, left and right knee	34
27	Clean spot inversion error, left ankle	35
28	Clean spot rotation error, right knee	36
29	Clean spot abduction error, left ankle	36
30	Phases of the gait cycle (Castermans et al. 2013)	38
31	Left Ankle Gait Curves	i
32	Left Knee Gait Curves	i
33	Left Hip Gait Curves	ii
34	Right Ankle Gait Curves	ii
35	Right Knee Gait Curves	iii
36	Right Hip Gait Curves	iii
37	Dirty spot calibration, boxplots left ankle	v
38	Dirty spot calibration, boxplots left knee	vi
39	Dirty spot calibration, boxplots left hip	vii
40	Dirty spot calibration, boxplots right ankle	viii
41	Dirty spot calibration, boxplots right knee	ix
42	Dirty spot calibration, boxplots right hip	x
43	Clean spot calibration, boxplots left ankle	xi
44	Clean calibration spot, boxplots left knee	xii
45	Clean calibration spot, boxplots left hip	xiii
46	Clean spot calibration, boxplots right ankle	xiv
47	Clean calibration spot, boxplots right knee	xv
48	Clean calibration spot, boxplots right hip	xvi

List of Tables

1	Inter segmental angles of MyoMotion Data according to ISB recommendations	19
2	Quantitative analysis of gait sequences, ordered by plane of motion .	23
3	Quantitative analysis of squats in dirty spot calibration trials, sagittal plane	27
4	Quantitative analysis of squats in dirty spot calibration trials, coronal plane	28
5	Quantitative analysis of squats in dirty spot calibration trials, transversal plane	30
6	Quantitative analysis of squats in clean spot calibration trials, sagittal plane	32
7	Quantitative analysis of squats in clean spot calibration trials, coronal plane	33
8	Quantitative analysis of squats in clean spot calibration trials, transversal plane	35
9	Offsets to Reference, Dirty Spot Calibration Trials	xviii
10	Offsets to Reference, Clean Spot Calibration Trials	xix

1 Introduction

1.1 Problem Definition

The usage of wearable inertial motion capture systems in the field of biomechanics has spread widely over the last years. Technological development made Inertial Measurement Units (IMU) a suitable application for human movement analysis such as the investigation of lower limb joint angles during gait (Iosa et al. 2016). Yet, despite their benefits over more expensive optical/markerbased systems, which are location-bound and often come with a laborious set up (W. Y. Wong, M. S. Wong, and Lo 2007), inertial sensor systems have other limitations.

While the sensor specific problems of accelerometers and gyroscopes, which are integrated noise and drift errors (Shull et al. 2014), can be dealt with in sensor fusion algorithms, integrated three-dimensional magnetometers are prone to disturbances of the earth magnetic field. This type of sensor is commonly used to define the initial alignment of the IMUs in a stationary, earth fixed reference frame (Favre et al. 2009) in a calibration process. With the known initial orientation of different sensors fixed to body segments, the IMUs are able to measure the movement of limbs and joint angles in between them.

However, inhomogeneous magnetic field conditions, which occur for example in indoor environments and in the proximity of ferromagnetic material, spoil the initial orientation of the sensors and lead to inaccurate or even completely wrong results (Laidig, Schauer, and Seel 2017). This decreases the usability of inertial motion capture systems, as it implies mapping the measurement volume to determine its ferromagnetic characteristics prior to the use of the system (De Vries et al. 2008), which is difficult to implement for clinics and motion labs.

1.2 Current Solutions

Since the use of magnetometer-instrumented IMUs is limited in the mentioned environment, researches and developers tried to implement Functional Calibration procedures, which require only IMU data (Favre et al. 2009; Laidig, Müller, and Seel 2017; Cooper et al. 2009; Lee and Jeon 2018). J. Favre proposed a functional calibration approach for the knee joint (Favre et al. 2009), Luinge et al used a similar

procedure for the elbow joint (Luinge, Veltink, and Baten 2007), as did Laidig et al in 2017 (Laidig, Müller, and Seel 2017).

The researchers approaches differed slightly, with some using a static and dynamic calibration, others like Cooper et al (Cooper et al. 2009) taking advantage of kinematic constraints, for which they for example simplified the knee joint as a hinge joint (Cooper et al. 2009; Lee and Jeon 2018).

1.3 Proposed Solution

All solutions presented show improved results when being compared to a reference system, but focus either on one single joint or are applied to rather artificially generated angles and were not evaluated in a purely biomechanical environment. In this study, two new approaches by the commercial manufacturer of inertial motion capture technology, Noraxon Inc. are validated. The Functional Calibration methods, referred to as Walking Calibration and Multipose, are accelerometer-based correction tools, which differ in their execution procedure and mathematical approach. Those methods were used to correct data of the lower limb human body angles, which was collected in a magnetically disturbed calibration spot by the Noraxon MyoMotion IMU system. In 10 trials with one healthy male subject, flexion, abduction and rotation angles of hip, knee and ankle in gait and squat movement were compared to a reference, which was defined by a marker-based motion capture system with eight infrared cameras by the company Qualisys. Besides, the methods were used on clean data in a magnetically homogeneous calibration space, to compare the behaviour of the Functional Calibration methods with the standard magnetometer based pose calibration, also in comparison to the marker-based reference.

1.4 Hypothesis

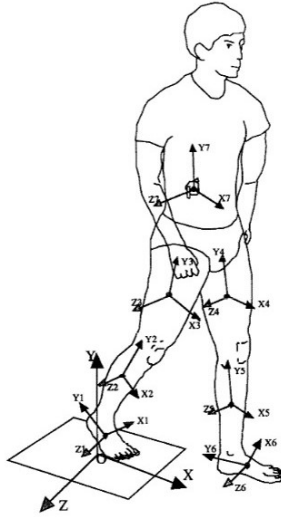
The Functional Calibration methods deployed by Noraxon are an approach to increase the usability of the MyoMotion System. Lower limb body angles in gait and squat are said to have minor deviations from the reference with both methods compared to the magnetically distorted standard calibration method. Furthermore, Walking Calibration and Multipose shall not deteriorate the clean data collected in the magnetically undistorted space.

2 Fundamentals

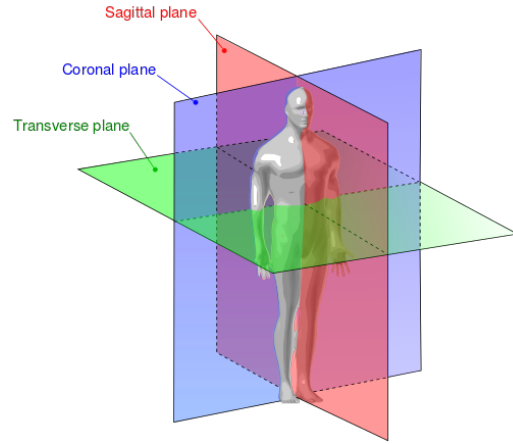
2.1 Planes of Human Motion

The conventions for a global reference frame for the reporting of kinematic data were proposed by the International Society of Biomechanics (ISB) in 1995 (Wu and Cavanagh 1995). The directions of movement along the 3 axes shown in Figure 1a are:

$$X\text{Axis} = \text{Forward/Backward} \parallel Z\text{Axis} = \text{Left/Right} \parallel Y\text{Axis} = \text{Up/Down}$$



(a) Conventions for global reference frame and segmental local center of mass reference frame (Wu and Cavanagh 1995)



(b) Human Planes
retrieved from (Bouza n.d.)

Figure 1: Planes of Human Motion

Three planes, namely sagittal, coronal and transversal, are assigned to the human body, as shown in Figure 1b. The axes of the reference frame lie within those planes. The X- and Y-axes lie in the sagittal plane, the X- and Z-axes lie within the transversal plane and the Y- and Z- axes in the coronal plane.

2.2 Anatomical terms of movement

The anatomical terms of movement of the lower limb are shown in Figure 2. *Flexion* is a movement in the sagittal plane, that decreases the angle between two body parts. Its contrary movement is *extension*. For the ankle, flexion is called *dorsiflexion*. *Abduction* is a movement in the coronal plane, away from the midline. *Adduction* means movement towards the line. The movement of a limb around their long axis is called *lateral* (or *external*) *rotation* for a movement away from the midline, *medial* (or *internal*) *rotation* for a movement towards the midline, both of which occur in the transversal plane. For the ankle, the internal rotation of the foot (sole point inwards) is called *Inversion*, the contrary movement is called *eversion*. It has to be noted that inversion occurs in the coronal plane, abduction of the foot in transversal plane. (TeachMeAnatomy 2015)

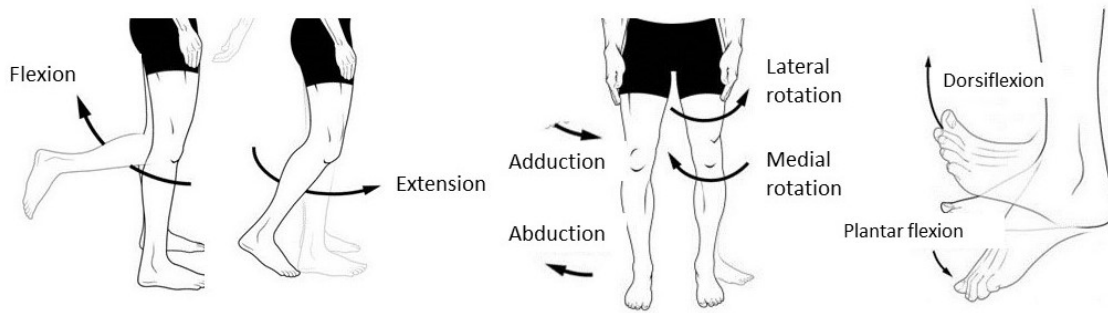
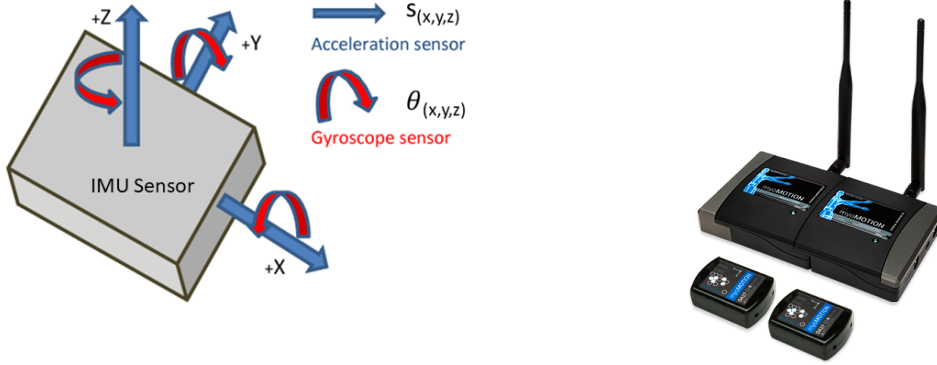


Figure 2: Anatomical Terms of Movement, adapted from (TeachMeAnatomy 2015)

2.3 IMU Technology

2.3.1 Sensor types

Inertial Measurement Units (IMU) consist of different sensor types, namely three accelerometers and three gyroscopes, each of which is mounted orthogonally to one another inside the mounting case. They provide measurement of translation S and rotation ϕ (Klein2004) along the axis of a sensor related 3D coordinate system, hereinafter referred to as sensor frame (Figure 3a). The axes of the sensor frame are shown on the mounting case (Figure 3).



(a) Translatory and Rotatory Degrees of freedom
Adapted from Kardos, Balog, and Slosarcik 2017

(b) MyoMotion Research Pro IMU,
Two Sensors and Receiver

Figure 3: Inertial Measurement Units

The x and y axis are printed on the sticker of the MyoMotion sensor. The z axis is pointing outwards perpendicular to the IMU surface.

The rotation of the sensor along the axes is described with the terms pitch, roll and course, similar to aviation technology. Course is the rotation around the x-axis, pitch is the rotation around the y-axis and roll the rotation around the z-axis. Additionally, three-dimensional magnetometers can be included in the sensor. This is the case in the "MyoMotion Research Pro IMU" (Figure 3b), which was used for this study.

Accelerometers

An accelerometer measures the force \vec{F} that acts on a mass m in the sensor across a single axis. Due to Newtons second law, acceleration a can be determined:

$$\vec{a} = \frac{\vec{F}}{m}$$

With a constant gravitation \vec{g} acting on the mass, the proper acceleration \vec{a}_p in the vertical axis is defined as:

$$\vec{a}_p = \vec{a} - \vec{g}$$

By integration of the acceleration, both velocity and distance along the vector can be calculated. Accelerometer signals are usually very noisy (Ferdinando, Khoswanto, and Purwanto 2012), which decreases the quality of integrated signals.

Gyroscopes

Gyroscopes measure a torque τ along one axis. With a given moment of inertia I , the angular acceleration vector α can then be defined as:

$$\alpha = \frac{I}{\tau}$$

Like accelerometer data, the angular acceleration has to be numerically integrated to obtain the desired angular position. With small, near constant deviations of the gyroscope data from the correct signal, the integration of those over time has a tendency to cause errors due to drift (Borenstein, Ojeda, and Kwanmuang 2009).

Magnetometers

Magnetometers are used to determine the magnetic north and by that the orientation of the IMU sensor. Electric magnetometers measure the Hall Voltage V , which will be induced by the Lorentz Force, which is a force that acts orthogonally on charge carriers of a current I located in an external magnetic field B (Oberlaender 2015). With d being the thickness of the conductor parallel to B and A_h the Hall coefficient, the magnetic field can be determined:

$$B = \frac{V \cdot d}{I \cdot A_h}$$

Magnetometers, like accelerometers and gyroscopes, are mounted orthogonally in the sensor housing to measure the orientation of the magnetic field in 3 axis.

2.3.2 Earth Frame and Progression Frame

To be able to make statements about the the course, pitch and roll orientation of sensors in respect of a stationary, earth fixed frame, this frame needs to be

determined in a calibration process. The system which describes the changes of those orientations is called attitude heading reference system (AHRS). The reference frame is hereinafter referred to as earth frame (Oberlaender 2015).

In a stationary position, the direction of the gravity vector, relative to the sensor, can be calculated with the information of the acceleration vectors as $\vec{a} = 0$ and therefore

$$\vec{a}_{p_x} + \vec{a}_{p_y} + \vec{a}_{p_z} = \vec{g}$$

The direction of the earth's frames vertical axis is the opposite of the direction of gravity (Figure 4).

To determine a horizontal axis, the distribution of the earth's magnetic field is measured in the three dimensional magnetometers (Oberlaender 2015), as well in a state of rest. This magnetic vector is however not pointing north in the horizontal plane, as the magnetic inclination has to be taken into account. Because of this, only the component of the magnetic field vector, which is perpendicular to the vertical axis, is taken as the north-pointing axis of the earth frame (Figure 4). The missing axis of the 3D earth frame coordinate system is determined mathematically and is pointing east.

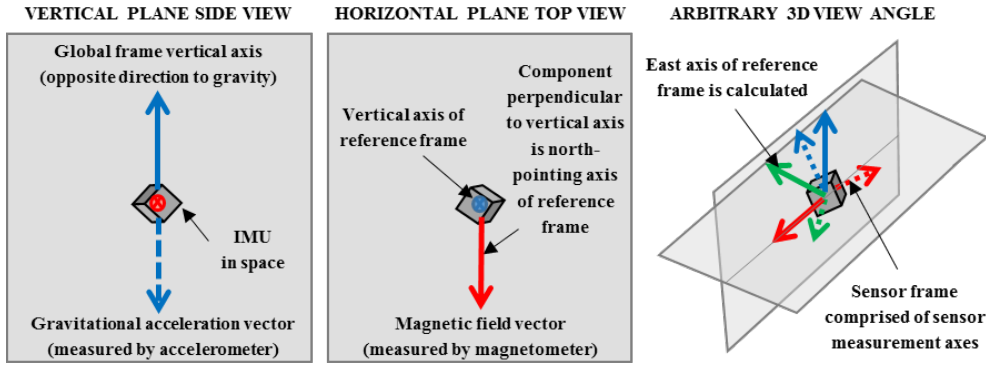


Figure 4: Attitude of the sensor in the earth frame (Cockroft 2015)

With the information obtained about the alignment of the sensor frame in the earth frame, the AHRS is defined. The MyoMotion System uses an adjusted reference frame, the so called progression frame, which basically is the earth frame rotated vertically. This adjustment gets the progression axis, which is the equivalent of the axis of the magnetic north, to point in a meaningful direction for human

progression. In the following, only the terms progression frame and progression axis are used.

2.3.3 Sensor Fusion

The data of IMUs is affected by its sensor limitations. In dynamic conditions, the acceleration signal is not dominated by the gravitational acceleration, so the attitude is predicted by the drift-prone information of the gyroscopes (Lee and Choi 2019). A method widely used to cope with those inaccurate measurements of IMU data is Kalman filtering.

A Kalman filter is an algorithm to predict the correct state of a system by fusing each sensor information, taking into account the previous time intervals. With this algorithm, value can be placed more on gyroscopes at high angular speed, but use the good long-term stability of accelerometers and, considering the magnetic homogeneity, the magnetometers (Michaelson 2018).

2.4 Posture Calibration of IMU based models

To estimate joint angles, it is necessary to measure the orientation of two adjacent body segments forming the joint (Vargas-Valencia et al. 2016). Alignment of sensors and their axes with the anatomical counterparts, however, is another issue related to IMU technology, as it is impossible to attach the sensors directly on the bones of each segment (Palermo et al. 2014; Seel, Raisch, and Schauer 2014). A standard method for estimating the body sensor alignment is the pose calibration (Morton, Baillie, and Ramirez-Iniguez 2013). Assuming that the segment has a rigid orientation relative to the sensor frame, the pitch, roll and course of each sensor is measured while the subject takes up an assumed posture. With sensors attached to the body segments of the lower limb including the pelvis, a standard calibration pose for the lower limbs is the standing upright posture or "soldier pose", which is displayed in Figure 5.

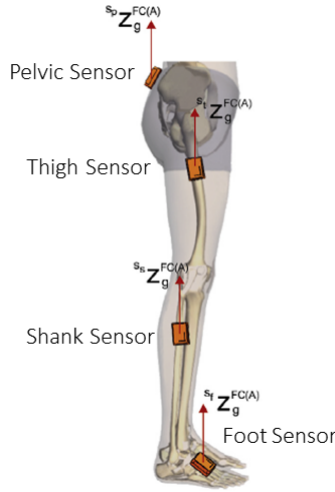


Figure 5: Alignment of the sensors with the lower limbs (Palermo et al. 2014)

This posture is also used as a standard calibration posture by the Noraxon MyoMotion IMU System. The sensors of the system have to be attached to the body with the x-axis of each sensor in the sagittal plane. The IMU-Model angles of the lower limb in this position are at 0° .

For a further understanding of the limitations of this calibration in inhomogeneous magnetic conditions, it must be mentioned that the progression axis used for the initial alignment of the sensor is calculated using the averaged magnetic north of all sensors. Yet, each sensor trusts its magnetic north to be correct, which in spoiled conditions creates random course orientation errors. Those run through an entire measurement, rendering them unusable.

2.5 Magnetic Field and Field Inhomogeneity

Correct calibration therefore depends on the fact that the magnetic north measured by the magnetometers is similar to the mean north and therefore no major differences between the horizontal earth vector orientations are given. Close to ferromagnetic material (for example iron), the earth magnetic field is not homogenous (Nowicki and Szewczyk 2015). This phenomenon affects measurements with magnetometers in buildings, as construction iron in floors, walls and ceilings affect the magnetic field. (De Vries et al. 2008)

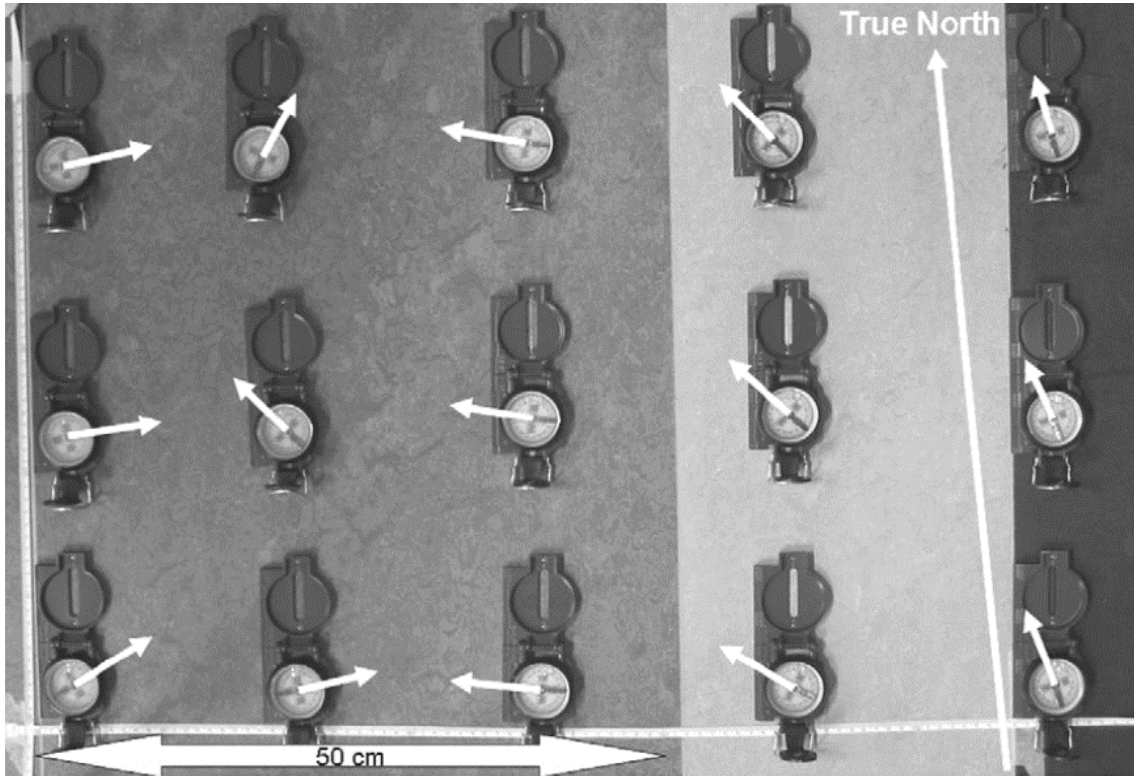


Figure 6: Qualitative Mapping with 15 identical compasses (De Vries et al. 2008)

W.H.K. de Vries et al. magnetically mapped a motion capture lab in 2008 with 15 identical compasses (see Figure 6). The figure shows the compasses on a floor, under which a solid iron construction was built to become a solid basis for some force plates. The compass needles (typically pointing north) all point in different directions, which shows the magnetic disturbance in this area.

2.6 Functional Calibration Methods

The term Functional Calibration method is typically used for procedures which determine the alignment of the sensors by movement, contrary to the static pose calibration (Morton, Baillie, and Ramirez-Iniguez 2013). With this more advanced calibration methods, the body segments are moved in predefined movements. These methods usually show better results, but need more time and expertise to carry out. The two new Functional Calibration procedures by Noraxon, which were validated in this study, follow a two step approach. The main goal was to suggest a method to

determine course orientation errors with the use of accelerometers and gyroscopes. The methods still use the static soldier pose described in subsection 2.4 for joint angle estimations. The procedures were designed to have a practical relevance for users, which is why assistance for the execution of movements was reduced to a minimum of markers on the ground for Walking Calibration and a stretch board for Multipose Calibration. The uncertainties of incorrect performances are consciously accepted in this study. In the following, the procedure and basic theoretical principles are explained.

2.6.1 Walking Calibration

To perform the Walking Calibration (WC), in the first step the subject is asked to stand in the soldier pose for a primary calibration. After the calibration is done, the subject walks in the direction he/she is heading. After about 5-10 meters, the subject turns around 180° and walks back to the calibration position. Once there, the subject turns around 180° again, so he/she is standing in the original calibration position. The movement is shown in Figure 7. The place where the initial pose was carried out should be marked on the floor for the subject to come back to the same position.

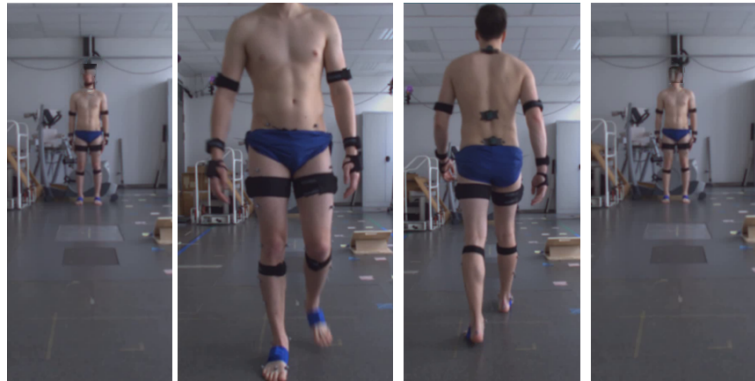


Figure 7: Walking Calibration Procedure

From left to right: Initial Position, walking in heading direction, turn around and walking in opposite direction, turn around back to initial position

By integration of the accelerometer data, considering the subtraction of the gravity component, the direction of movement of each sensor can be determined. With

spoiled progression axes, each sensor would translate in a different direction while walking. Functional Walking Calibration exploits the fact that the sensors mounted on the body segments should move in the same direction over time and can therefore correct the course orientation error of each sensor. With the drift-prone integration signals of the IMUs, the signals are however not accurate. To compensate this, the initial and final condition of the calibration will be taken into account and a pure forward/backward floor translation is assumed. The procedure is guided by a wizard in the Noraxon MR Software which gives feedback on correct execution.

2.6.2 Multipose

Like the first calibration step of the Walking Calibration, for the Multipose Calibration (MP) the subject needs to stand in the soldier pose for the initial calibration. After that, the subject bends forward with a straight back for about 20 to 30°. Following, the subject is asked to elevate the legs one after the other with a stiff knee and keep it still after that. In both movements, the focus lays more on movement only in the sagittal plane and avoidance of rotation or abduction movements, rather than raising or bending for an exact ankle. To make the performance of the movement easier, a stretch board can be used. In Figure 8 the different positions of the calibration procedure are shown.

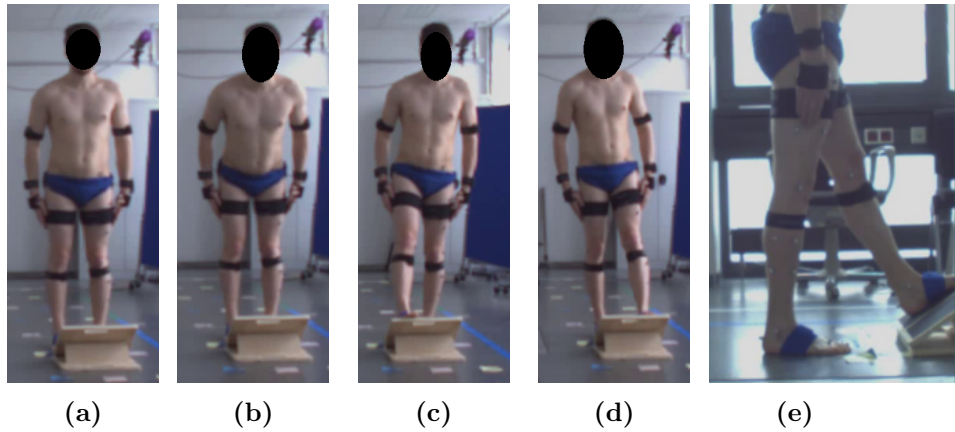


Figure 8: Steps of Multipose Calibration (a)-(e)

Performed on a stretch board (a) shows the Subject standing in the soldier pose, in (b) the subject bends over, (c) shows the right leg raise, (d) the left leg raise in anterior view and (e) in lateral view

The theoretical approach of this calibration procedure is similar to the one proposed by Eduardo Palermo et al. 2014. The idea behind it is to observe the gravitation vector $\vec{g}1$ in the soldier pose and the second gravitation vector $\vec{g}2$ in the second pose. If the sensor rotates around an axis parallel to the ground, the gravity vectors will remain in a plane perpendicular to that axis. With the assumption of movement of each sensor within its own sagittal plane, the plane can then be determined because both vectors $\vec{g}1$ and $\vec{g}2$ lie in the sagittal plane. The progression axis therefore must be in the sagittal plane and perpendicular to $\vec{g}1$. Each sensors' course error can thus be exposed and corrected. The bending posture provides the $\vec{g}2$ information for the pelvis sensor, the leg movements for the sensors on thigh, shank and foot on each side.

3 Materials and Methods

3.1 Test Procedure

The IMU Calibration Methods were validated against an optical reference system by comparing the body angles of the lower extremities during gait and squat movement for initial calibration in a magnetically inhomogeneous spot. In a second test sequence, calibration methods were validated for the squat movement for an initial calibration spot with presumed magnetic homogeneity. The measurement consisted of a predefined movement sequence. First the IMU-Model was calibrated when the subject was in the soldier pose. Straight after, the subject performed the Walking Calibration as described in 2.6.1. After finishing the procedure, the subject walked towards the middle of the measuring volume of the optical system and performed a squat movement. After that, the subject performed the Multipose Calibration (2.6.2). Attention was paid to ensure that the subject faced the same direction as in the initial calibration. All of the movements were performed barefoot. The measurement setup is schematically shown in Figure 9.

IMU data and reference data were collected simultaneously. The systems were synchronized by a synchronization unit, which sent an analog trigger signal. The IMU system acted as master, the optical system as slave. Both measurement systems recorded with 100 Hz. The measurement was also recorded by two Ninox 300C cameras (Noraxon Inc, Scottsdale, Arizona) at 100 frames per second, which were also synchronized by the synchronization unit.

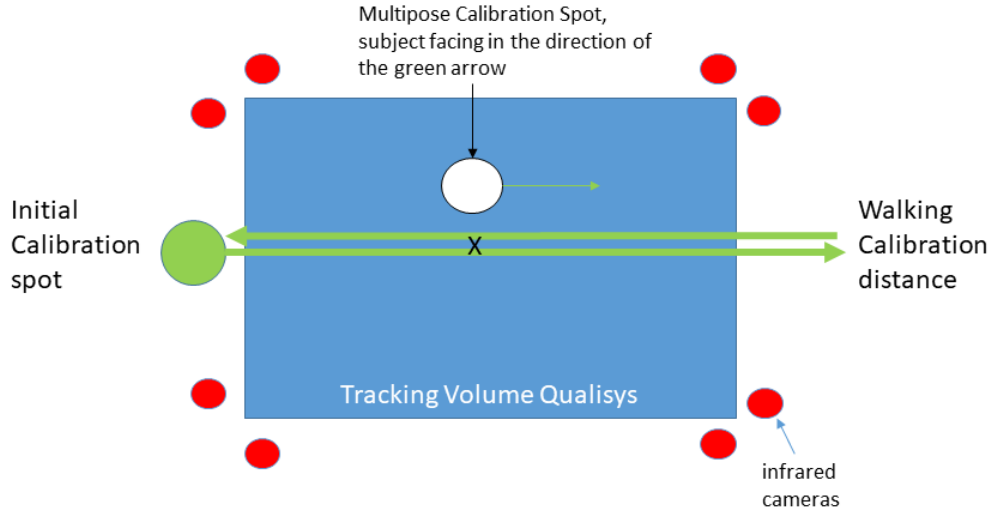


Figure 9: Measurement setup

The Walking Calibration distance exceeds the tracking volume of the Qualisys system.

3.2 Subject and Material

The measurement took place in a motion analysis laboratory at the German Sports University Cologne. One healthy male subject (185cm, 82 kg), who gave his agreement to participate in this study, performed ten trials with an initial calibration in a magnetically disturbed place, based on information by the IMU system, and ten trials with an initial calibration in a magnetically clean place. The subject had performed both Functional Calibration procedures in some preliminary tests under different conditions before the day of measurement.

3.2.1 IMU System

The IMU system used was the MyoMotion Research Pro IMU with the Firmware 5.16 (Noraxon Inc, Scottsdale, Arizona) with 7 sensors attached to the pelvis, thigh (left/right), shank (left/right) and the bare foot(left/right). Specifications of the sensors can be found in the attached brochure. The sensors were fixated with straps

provided by Noraxon. The foot sensors were attached with tape (Figure 10). Data was transferred wirelessly and processed by the software MyoResearch Developer Version 3.15 (MR3, Noraxon Inc, Scottsdale, Arizona).



Figure 10: Subject with attached sensors and CAST marker set

3.2.2 Reference System

Optical motion capture systems use infrared cameras to capture the position of retroflective markers attached to the skin in an initially calibrated tracking volume. The joint angles are derived from anatomical models. Those are created by preparing the subject with specific marker sets, of which there are many different ones available. The subject has to be recorded in the soldier pose for an initial static trial to record the markers, which are attached to anatomical landmarks, to create the anatomical model. The accuracy of optical systems has been evaluated many times and they are commonly referred to as the gold standard in biomechanical motion capture technology (Kruk and Reijne 2018).

Eight infrared cameras (500 / 510 +, Qualisys AB, Göteborg, Sweden) were used to track 36 retroflective markers with the Software Qualisys Track Manager (QTM, Qualisys AB, Göteborg, Sweden). The tracking volume was calibrated prior to the measurement statically and dynamically as recommended by the company. The markers were attached to anatomical landmarks according to the Calibrated

Anatomical Systems Technique (CAST) lower body marker set (Cappozzo et al. 1995) with adhesive tape (Figure 10, Figure 11). The operator was instructed by an experienced examiner before the measurement. QTM provides an Automatic Identification of Markers (AIM) algorithm to assign the markers in the software to the body parts. Possible gaps were filled manually by the operator.

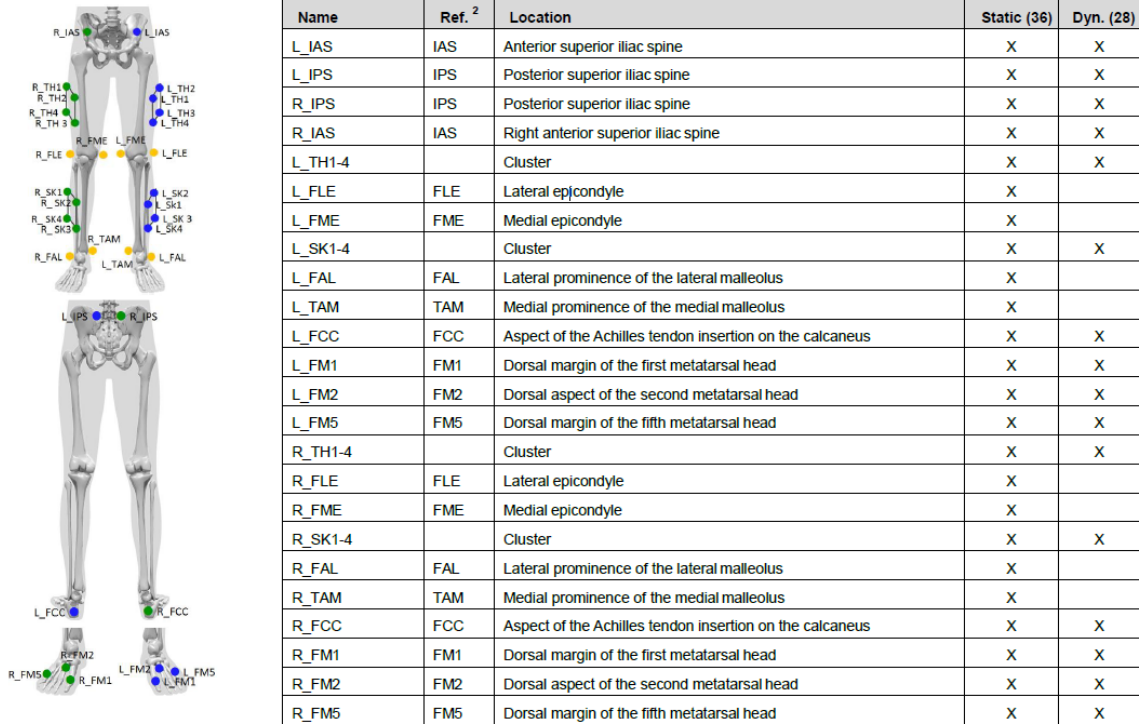


Figure 11: Position and labels of markers for the CAST marker set

3.3 Calibration Spots

The magnetically disturbed place (dirty spot) was created by putting a bicycle ergometer directly next to the subject while performing the initial calibration. The ergometer is built with a lot of ferromagnetic material. The clean spot was on a plastic stool, elevating the subject from eventual construction iron in the floor. The magnetic (in-)homogeneity is indicated by the magnetometer table in the MR3 Software (Figure 12).

The columns represent:

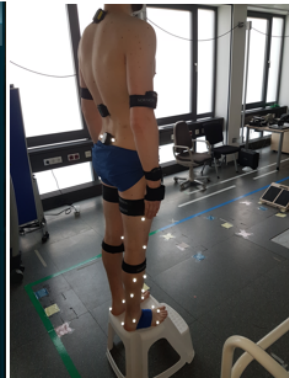
1. The magnetic vector strength normalized to the vector strength at the place of factory calibration in Scottsdale, Arizona
2. Its difference to the reference vector, calculated over all vectors.
3. The dip angle between the magnetic inclination and gravity.
4. Its difference to the reference angle, calculated over all sensors.

Sensor	L	Δ	$^\circ$	Δ
Ref	0.965		60.5	
Pelvis	1.183	0.218	51.4	-9.1
Lower Thoracic	1.197	0.233	59.5	-0.9
Upper Thoracic	1.057	0.092	65.2	4.7
Left Upper Arm	1.036	0.072	66.7	6.3
Left Forearm	0.810	-0.155	59.7	-0.8
Left Hand	0.745	-0.220	57.1	-3.4
Left Thigh	0.688	-0.277	53.6	-6.8
Left Shank	0.960	-0.005	53.2	-7.2
Left Foot	1.046	0.081	63.7	3.2
Right Upper Arm	1.033	0.068	63.4	3.0
Right Forearm	0.877	-0.087	57.6	-2.9
Right Hand	0.822	-0.143	58.1	-2.3
Right Thigh	0.771	-0.194	55.4	-5.0
Right Shank	0.886	-0.079	55.8	-4.7
Right Foot	1.712	0.747	68.0	7.5



(a) inhomogeneous spot in front of ergometer

Sensor	L	Δ	$^\circ$	Δ
Ref	0.993		65.0	
Pelvis	1.008	0.015	64.9	-0.1
Lower Thoracic	1.006	0.013	65.3	0.3
Upper Thoracic	1.033	0.040	64.1	-0.9
Left Upper Arm	1.004	0.011	63.2	-1.8
Left Forearm	0.982	-0.011	63.2	-1.8
Left Hand	0.956	-0.037	61.9	-3.1
Left Thigh	0.950	-0.043	64.5	-0.5
Left Shank	0.942	-0.051	65.0	-0.0
Left Foot	0.988	-0.005	66.8	1.8
Right Upper Arm	1.033	0.040	66.0	1.0
Right Forearm	0.992	-0.001	65.7	0.7
Right Hand	0.980	-0.013	66.2	1.2
Right Thigh	0.958	-0.035	64.4	-0.6
Right Shank	0.942	-0.051	65.9	0.9
Right Foot	0.984	-0.009	64.8	-0.2



(b) clean spot on plastic stool

Figure 12: Calibration spots with magnetometer table

Essentially, the reference values (first row) are calculated by eliminating outliers, to reduce the risk of a badly disturbed sensor to spoil the result, and then finding the average of the non-outliers. Sensors are then displayed red if their vector strength- or dip angle difference is above a certain threshold which is set by Noraxon. The magnetometer table in 12(a) shows a heavily disturbed spot. Noraxon usually rec-

ommends not to calibrate the MyoMotion System with the standard pose calibration in such an area. It has to be mentioned though, that the magnetic dip angle only shows inhomogeneity in the vertical plane, which is irrelevant for the determination of the earth frame (subsubsection 2.3.2). The differences are more to be seen as a note to inhomogeneity also in the horizontal plane.

3.4 Data Acquisition

The MyoMotion data was split into three data sets for each trial. The data was recorded with the Walking Calibration (WC) instruction wizard, which detects the WC-Procedure automatically. In MR3, the Calibration can then manually be set back to the default pose calibration (Restored Metrics) in the dirty or clean spot. The Multipose (MP) Calibration was applied manually by picking frames in the NiNOX 300C video of the procedure post-hoc. The poses were detected by the operator for each leg and the spine as described in 2.6.2. Each MyoMotion model outputs cardan angles to describe angular kinematics for the skeletal joints and segments. The angles definitions based on recommendations of the ISB are shown in Table 1.

Name	Anatomical axes	Cardan Sequence	Range	Polarity (positive)
Hip	X - flexion Y - rotation ext Z - abduction	XZ'Y''	X: [-180 180] Y: [-180 180] Z: [-90 90]	Hip Flexion Hip Rotation Ext Hip Abduction
Knee	X - flexion Y - rotation ext Z - abduction	XZ'Y''	X: [-180 180] Y: [-180 180] Z: [-90 90]	Knee Flexion Knee abduction Knee rotation Ext
Ankle	X - dorsiflexion Y - abduction Z - inversion	XY'Z''	X: [-180 180] Y: [-90 90] Z: [-180 180]	Ankle Dorsiflexion Ankle Abduction Ankle Inversion

Table 1: Inter segmental angles of MyoMotion Data according to ISB recommendations

With the Project Automation Gait Visual3D Module (Version 1.4.0.54) in the QTM software, the optical reference data was processed to Visual 3D (Version 6.03.6, C-Motion Inc, Germantown, Maryland), in which angle calculations were executed. Built-in event detection for gait cycles, using the algorithm described by Zeni Jr, Richards, and Higginson 2008, was used to determine heel strike timestamps for the gait cycles. Squat detection was done manually by the operator by detecting the

start of the movement in the NiNOX 300C video. The data was then exported to an ASCII file.

As system assumptions or different anatomical model calculations of the different motion analysis systems can lead to different quantitative angle data (Ferrari et al. 2008; Kainz et al. 2016), the system values were brought into line by eliminating constant offsets. This approach is common in biomechanics, as the original data would suggest that the systems vary a lot, but are not indicative of the angle waveform. The offset of each MyoMotion data set was calculated from the average offset value of each set compared to the Reference data set. The offset values are attached in the appendix.

3.5 Data Analysis

The datasets were rearranged for each joint angle side by side according to their timestamp in Microsoft Excel (MS Excel 2013, Microsoft Corp. , Redmond, Washington). Afterwards, analysis was done in the Matlab Environment (Version R2020a, The MathWorks Inc. Natick, Massachusetts). The squats of each trial were treated as individual data sets. In order to check the repeatability, the gait cycles of all 10 dirty spot measurements were combined into one data set for each calibration method, by calculating the mean and standard deviation of the gait curves for every point in time starting from the heel strike. It was paid attention to gaps in the data. For the left leg 57 steps and for the right leg 55 heel strikes could be detected in Visual 3D. Since not all gait cycles were captured completely by the optical reference system, which is limited by its tracking volume, the cycles were not normalized over time.

3.6 Statistical Analysis

All data sets were plotted over time and qualitatively evaluated.

The gait cycles were plotted with one standard deviation (STD). The mean of the standard deviations (mSTD) was calculated to evaluate the repeatability.

Quantitative analysis consisted of the comparison of the root-mean-square error (RMSE) of each calibration method. RMSE of a data set x_1 compared to the reference x_2 with the lengths i is generally calculated as following:

$$RMSE = \sqrt{\frac{1}{n} \sum_{i=1}^n (x_{1,i} - x_{2,i})^2}$$

The RMSE of each data set was also normalized (nRMSE) to the reference Range of Motion (ROM) of each movement.

$$nRMSE = \frac{RMSE}{ROM}$$

Range of Motion analysis was performed for all squat trials. The ROM of each movement is the difference between the minimal and maximal joint angle value.

The error between each Functional Calibration method and the reference in squat movements was visualized with boxplots. Boxplots show the distribution of data. The Median, the approximate (first and third) quartiles and outliers are displayed. This gives information about the range and symmetry of the Error-Values. (Figure 13)

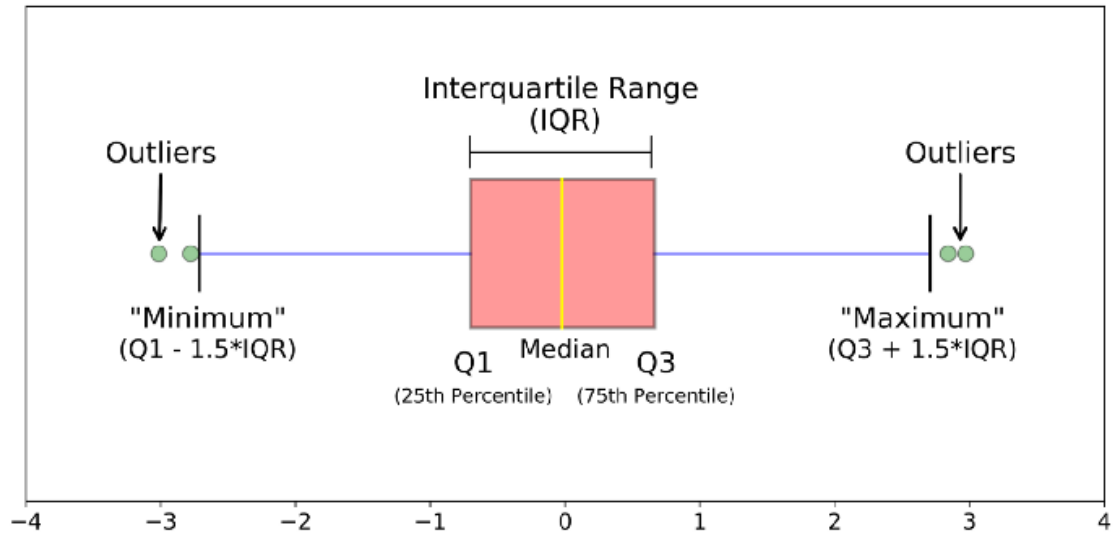


Figure 13: Definition and explanation of a boxplot, from Galarnyk 2018

4 Results

4.1 Dirty Spot Calibration

4.1.1 Gait

Quantitative results of the gait trials can be found in Table 2. The results were split for each plane of human motion. The mean standard deviation of the curves varied between 1.37° and 3.62° .

Sagittal Plane

In the sagittal Plane, RMSEs for MP (1.29° - 2.38°) and WC (0.92° - 2.50°) was better then for Restored dirty spot calibration (4.46° - 5.69°) in knee and ankle joint. The hip joint shows equal results for all calibration methods varying between 0.98° - 1.72° . The maximum error of both Functional Calibration methods was below 5° for all joints, the Restored Metrics produced higher errors for the averaged gait in knee and ankle joint data.

All curves were similar and showed no abnormalities apart from the deviations mentioned. Figure 14 shows representatively the curves for left ankle and right knee.

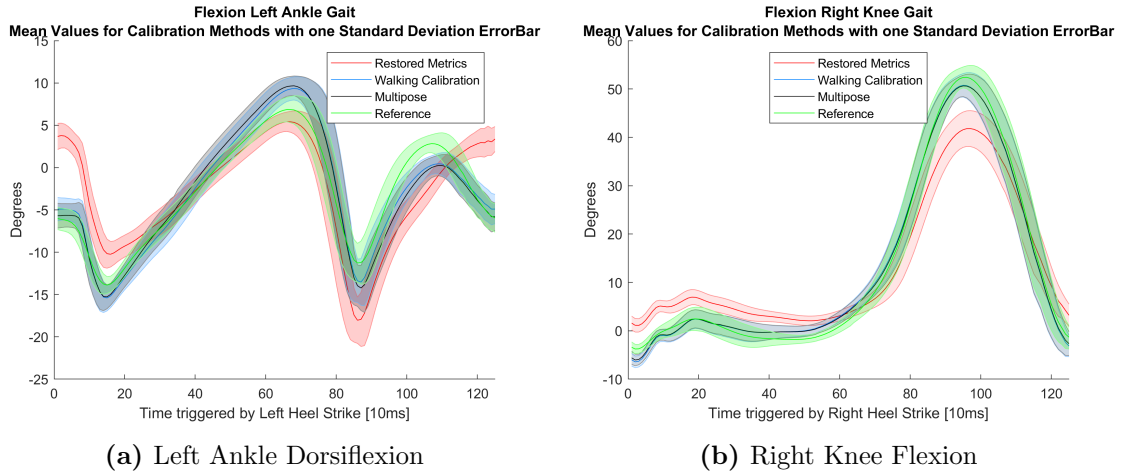


Figure 14: Gait curves, sagittal plane

Positive values represent flexion respectively dorsiflexion, negative values extension/plantar flexion

Sagittal Plane

Body Joint	ROM(°) Reference	RMSE						STD			maxerror (°)	
		mRMSE (°)			nRMSE (%/ROM)			mSTD (°)				
		WC	MP	Restored	WC	MP	Restored	WC	MP	Restored	WC	MP
Left Ankle Flexion	20,74	1,75	2,07	4,46	8,44	9,97	21,52	2,17	2,11	2,05	3,20	3,15
Right Ankle Flexion	20,30	2,50	2,38	5,69	12,32	11,74	28,00	2,05	2,00	2,55	3,79	4,08
Left Knee Flexion	57,64	0,92	1,29	5,45	1,60	2,24	9,45	3,01	2,98	2,64	1,36	1,36
Right Knee Flexion	56,17	1,43	1,30	5,54	2,55	2,31	9,86	3,06	3,04	2,68	2,06	1,86
Left Hip Flexion	32,77	1,06	0,98	1,03	3,25	3,01	3,14	1,94	1,79	1,79	2,21	1,90
Right Hip Flexion	30,96	1,72	1,52	1,23	5,55	4,91	3,97	2,00	1,72	1,74	2,42	2,09

Coronal Plane

Body Joint	ROM(°) Reference	RMSE						STD			maxerror (°)	
		mRMSE (°)			nRMSE (%/ROM)			mSTD (°)				
		WC	MP	Restored	WC	MP	Restored	WC	MP	Restored	WC	MP
Left Ankle Inversion	7,55	2,72	1,89	11,31	36,04	25,02	149,88	2,46	2,74	2,98	6,12	2,84
Right Ankle Inversion	10,92	1,92	4,67	4,38	17,57	42,77	40,15	2,57	3,20	2,21	3,14	10,26
Left Knee Abduction	5,81	2,90	1,62	14,31	49,88	27,90	246,46	1,59	1,77	2,16	4,04	2,96
Right Knee Abduction	6,76	1,93	3,42	14,05	28,57	50,54	207,84	3,06	3,04	2,68	3,63	6,46
Left Hip Abduction	8,03	1,31	1,19	2,46	16,28	14,81	30,59	1,78	1,81	1,37	2,79	2,40
Right Hip Abduction	8,43	1,63	0,95	2,60	19,35	11,32	30,87	1,50	1,64	1,52	3,34	2,25

Transversal Plane

Body Joint	ROM(°) Reference	RMSE						STD			maxerror (°)	
		mRMSE(°)			nRMSE (%/ROM)			mSTD(°)				
		WC	MP	Restored	WC	MP	Restored	WC	MP	Restored	WC	MP
Left Ankle Abduction	12,47	2,31	3,18	2,78	18,51	25,54	22,33	2,33	2,10	2,01	4,70	4,78
Right Ankle Abduction	10,70	2,50	2,38	5,69	23,37	22,26	53,13	2,05	2,00	2,55	4,28	5,56
Left Knee Rotation	7,80	3,25	3,85	1,66	41,61	49,29	21,30	2,83	2,18	2,18	5,65	7,59
Right Knee Rotation	11,87	3,91	4,64	7,01	32,92	39,07	59,08	2,92	3,62	3,52	7,72	9,51
Left Hip Rotation	14,60	1,92	2,06	2,39	13,14	14,13	16,34	2,46	1,89	1,88	2,63	2,75
Right Hip Rotation	11,84	2,47	2,18	1,69	20,81	18,37	14,29	3,48	2,26	2,28	3,16	2,84

Table 2: Quantitative analysis of gait sequences, ordered by plane of motion

Coronal Plane

The RMSE for movements in the coronal plane ranged from 1.31° - 2.90° for WC and 0.95° - 4.67° for MP to 2.60° - 14.31° for the Restored Metrics. The functional calibration methods showed better results then the Restored Metrics, with the most significant difference in knee abduction, where the nRMSE of the spoiled data could be reduced from more than 200 % to about 28-50 %.

Inversion error for both ankles was at the lowest for WC. A remarkably high RMSE of 11.31° in the restored ankle inversion for the left side was reduced by MP and WC, for the right ankle Multipose RMSE was at similar level (4.67°) as the restored metrics (4.38°). The maximal errors were higher for the Restored Metrics in each hip and knee joint. Maximal errors for WC exceeded 5° only for the left ankle inversion, Multipose exceeds 5° error for the right ankle and right knee.

Abduction curves of both hip joints correlated over the whole cycle. Abduction curves of WC and MP were similar for the knee joint, restored metrics resulted in completely spoiled data (Figure 15).

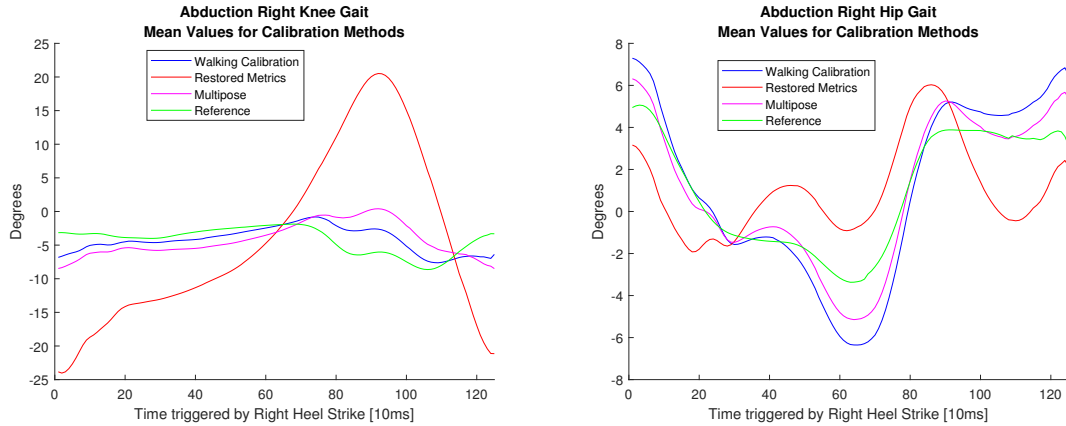


Figure 15: Gait curves, right knee and right hip abduction
Positive values represent abduction, negative values adduction.

While inversion curves of the left angle were similar for WC, MP and Reference, rotation of the right ankle was indicating an inversion peak at about 90 seconds for MP, while WC and Reference did not indicate this peak. Restored metrics showed different results for both ankles (Figure 16).

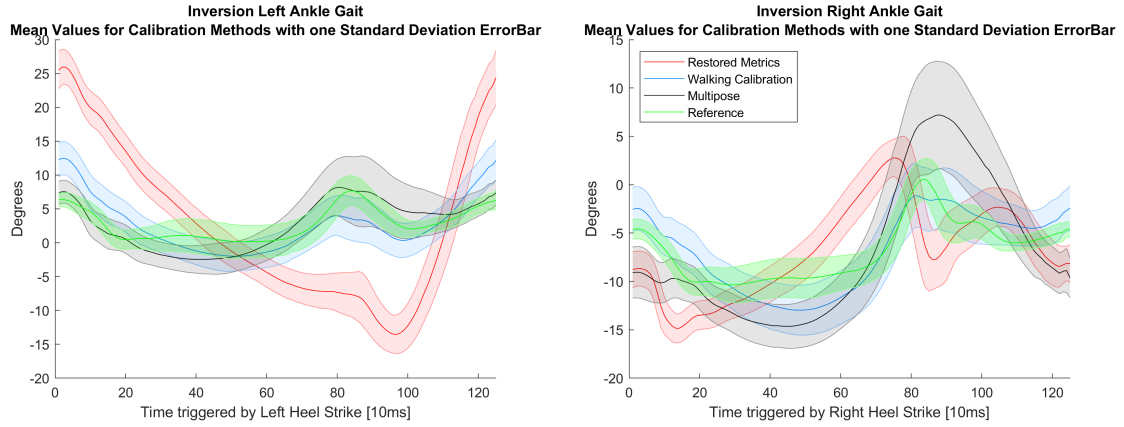


Figure 16: Gait curves, ankle inversion
Positive values represent inversion, negative eversion.

Transversal Plane

For abduction of the ankle, the Multipose RMSE (3.18°) was worse than the original Restored Metrics value (2.78°). Static calibration in the dirty spot showed better results for the left knee than the functional calibration methods. The Restored Metrics RMSE for the right knee was higher than with the Functional Methods. Hip rotation of both sides showed similar results for all methods.

Both ankle curves showed a similar curve for the abduction except a deflection of the IMU data curves at about 90 seconds, which is reflected in larger deviations (Figure 17). The deflections of MP and WC indicate adduction of the ankle, whereas the Restored Metrics suggest an abduction movement at this time. In Figure 18 the correlating rotation for the left hip and for the left knee with the deflection are displayed.

The IMU rotation curves of both hips correlated with the reference over the whole gait cycle, yet the standard deviation was higher than the one of the reference. In the rotation curves for both knees, IMU sensors indicated an external rotation at about 90-100 seconds after the heel strike, which was not indicated by the reference. Other than that, the curves correlated.

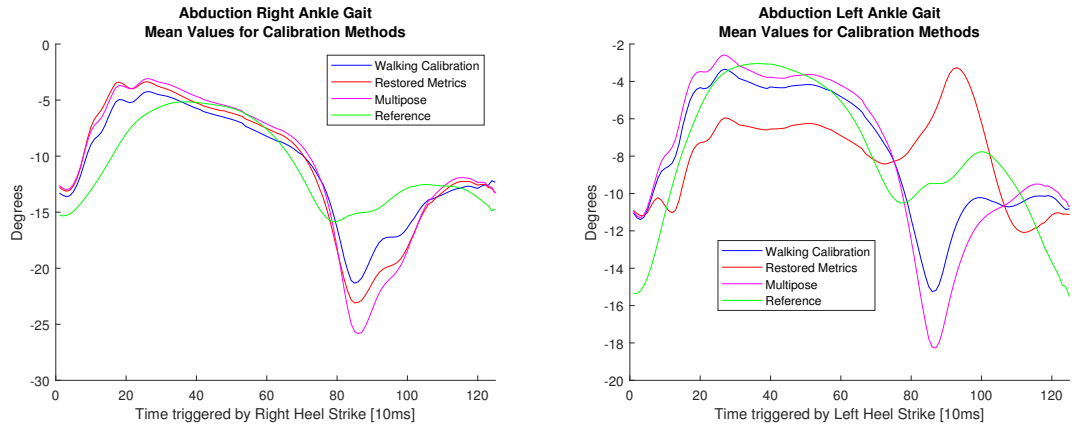


Figure 17: Gait curves, right and left ankle abduction
Positive values represent abduction, negative values adduction.

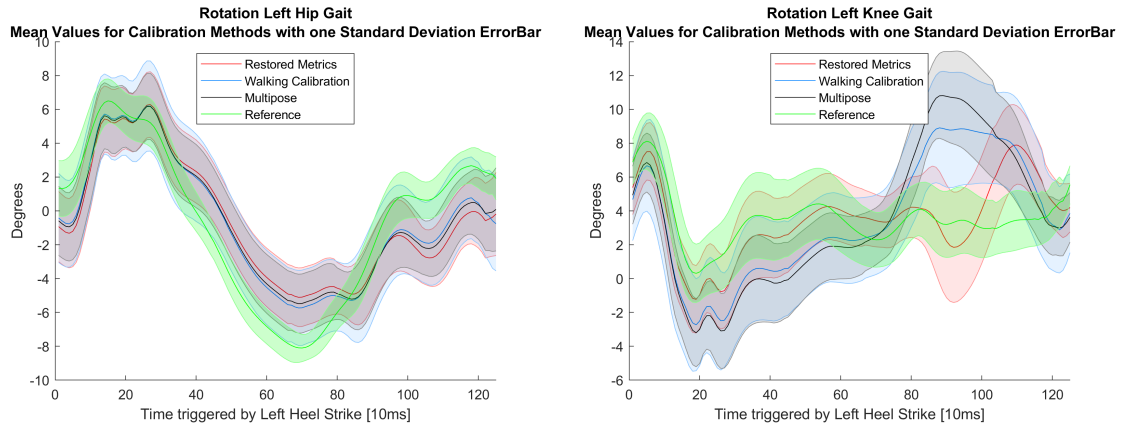


Figure 18: Gait curves, left hip and knee rotation
Positive values represent abduction, negative values adduction.

4.1.2 Squats

In the following, only quantitative values averaged over all trials and representative measurement results are presented. The error boxplots of all trials can be found in the appendix.

Sagittal Plane

The RMSE and ROM averaged over all trials are shown in Table 3.

Sagittal Plane						
	Left Hip	Right Hip	Left Knee	Right Knee	Left Ankle	Right Ankle
RMSE (mean \pm std in $^{\circ}$)						
WC	2,57 \pm 0,37	2,08 \pm 0,28	1,98 \pm 0,24	2,33 \pm 0,20	2,80 \pm 0,36	2,58 \pm 0,24
MP	2,58 \pm 0,40	2,14 \pm 0,29	2,15 \pm 0,29	2,21 \pm 0,23	3,98 \pm 2,86	2,46 \pm 0,32
Restored	2,41 \pm 0,33	2,11 \pm 0,32	4,32 \pm 0,81	5,01 \pm 1,03	6,02 \pm 0,49	5,98 \pm 0,74
ROM (mean \pm std in $^{\circ}$)						
Reference	63,0 \pm 3,89	59,3 \pm 4,16	86,6 \pm 3,13	81,5 \pm 2,88	35,2 \pm 1,46	34,6 \pm 1,60
WC	68,0 \pm 5,12	62,4 \pm 5,63	81,4 \pm 2,91	75,8 \pm 2,96	29,2 \pm 1,95	29,4 \pm 2,13
MP	67,9 \pm 5,15	62,7 \pm 5,20	81,1 \pm 2,81	76,1 \pm 2,98	26,6 \pm 7,25	29,7 \pm 2,16
Restored	67,4 \pm 5,03	62,6 \pm 5,38	75,6 \pm 4,39	69,1 \pm 5,65	20,4 \pm 1,59	21,2 \pm 3,20

Table 3: Quantitative analysis of squats in dirty spot calibration trials, sagittal plane
The mean and standard deviation was calculated over all 10 trials.

The hip joint RMSE and ROM of the IMU Data did not differ much. RMSE was between 2.08°-2.58° and the ROM between 105.22% -107.94% of the Reference ROM. For the knee and hip joints, the functional calibration methods increased the RMSE and ROM/Reference-ROM compared to Restored Metrics for both sides. Neither method gave significantly better results than the other, but there was an outlier in trial 5 for the left ankle in MP calibration, which influences the mean values and STD. The left ankle flexion error is shown in Figure 19 exemplary. For all other joints, no outliers were detected.

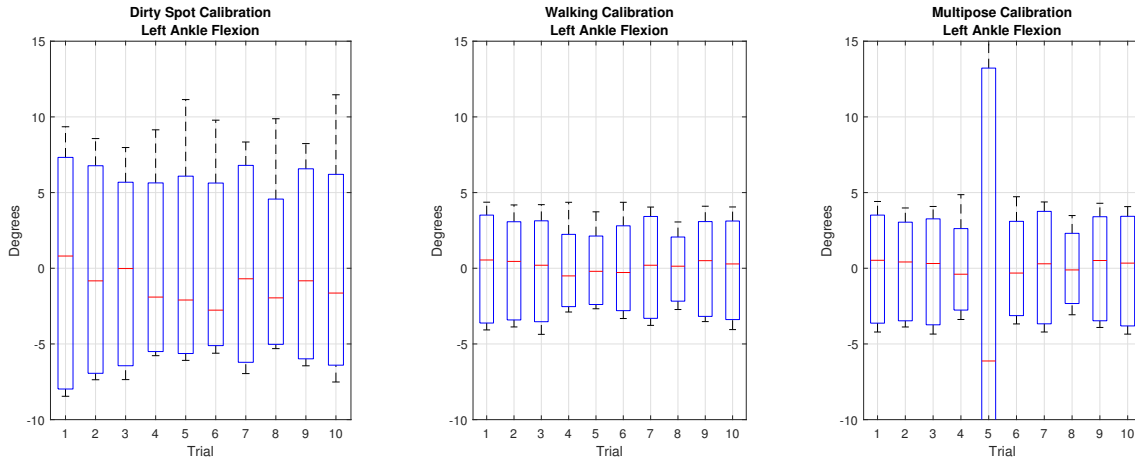


Figure 19: Dirty spot dorsiflexion error, left ankle
Walking Calibration and Multipose minimized the error to values lower than $\pm 5^\circ$. Trial 5 showed spoiled results for the left ankle.

Coronal Plane

The RMSE and ROM averaged over all trials are shown in Table 4.

Coronal Plane						
	Left Hip	Right Hip	Left Knee	Right Knee	Left Ankle	Right Ankle
RMSE (mean \pm std in $^\circ$)						
WC	$1,52 \pm 0,94$	$1,25 \pm 0,62$	$3,95 \pm 1,42$	$1,47 \pm 1,00$	$0,82 \pm 0,28$	$2,28 \pm 0,42$
MP	$1,87 \pm 0,82$	$0,93 \pm 0,52$	$2,05 \pm 1,03$	$2,39 \pm 1,17$	$2,70 \pm 0,62$	$3,76 \pm 1,29$
Restored	$2,25 \pm 0,48$	$4,06 \pm 0,56$	$14,1 \pm 1,15$	$13,4 \pm 1,57$	$8,01 \pm 0,62$	$10,0 \pm 0,67$
ROM (mean \pm std in $^\circ$)						
Reference	$4,00 \pm 0,98$	$7,10 \pm 0,92$	$9,00 \pm 0,50$	$5,79 \pm 0,60$	$5,62 \pm 1,44$	$5,06 \pm 1,34$
WC	$7,38 \pm 2,22$	$8,37 \pm 3,28$	$5,27 \pm 1,61$	$6,35 \pm 2,58$	$4,85 \pm 1,20$	$7,56 \pm 1,42$
MP	$7,62 \pm 1,31$	$8,44 \pm 2,13$	$6,83 \pm 2,94$	$5,53 \pm 3,28$	$7,16 \pm 1,05$	$11,3 \pm 3,09$
Restored	$9,31 \pm 1,70$	$6,58 \pm 1,93$	$28,1 \pm 2,05$	$32,4 \pm 4,19$	$23,7 \pm 2,29$	$25,8 \pm 1,85$

Table 4: Quantitative analysis of squats in dirty spot calibration trials, coronal plane
The mean and standard deviation was calculated over all 10 trials.

Significant improvements could be detected for knee abduction, with a mean Range of Motion of $28,1^\circ/32,4^\circ$ for Restored Metrics, which is more than five times higher than the reference. Mean ROM for WC/MP is at 110/96% of the Reference ROM for the right knee and 59/76% for the left knee. Errors exceeded $\pm 5^\circ$ only in trial 10 and for multipose in trial 7 and 9 (Figure 20).

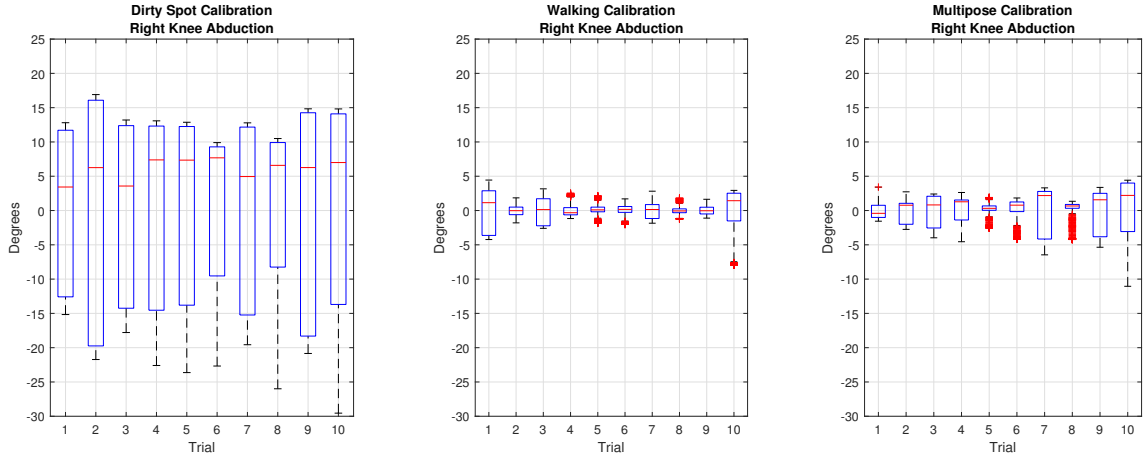


Figure 20: Dirty spot abduction error, right knee
Walking Calibration and Multipose significantly reduce the dirty spot calibration Error, Q1 and Q3 are always below 5°.

The mean RMSE for the hips was lower for both functional calibration methods, with the lowest score of 0.93° (Right Hip, Multipose Calibration). Error boxplots are shown in Figure 21.

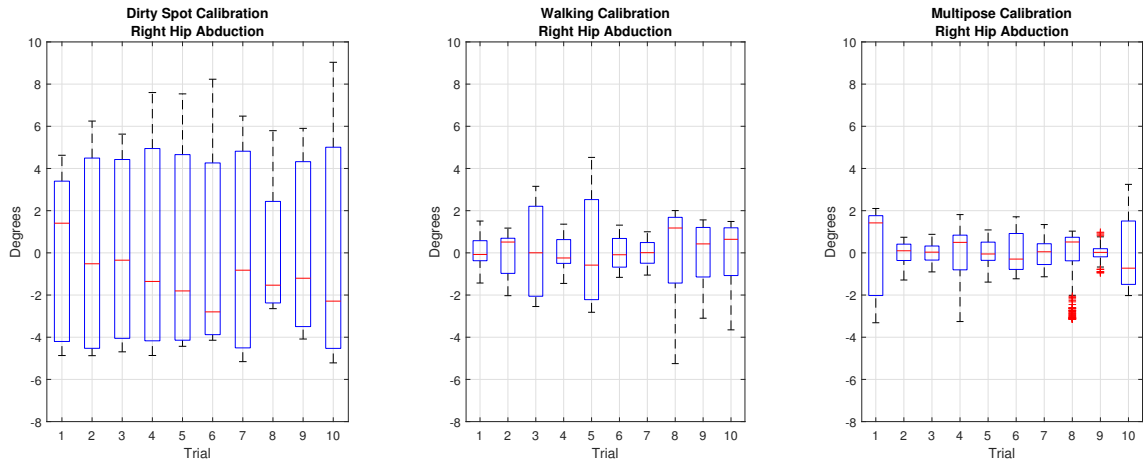


Figure 21: Dirty spot abduction error, right hip
Walking Calibration and Multipose show maximum errors for all trials lower than 5°

MP and WC showed better results for both ankles, decreasing the RMSE of the static pose calibration from 8.01/10° to less than 4°. WC showed the lowest RMSE for the ankle inversion and also had the smallest difference of ROM to the Reference

ROM. The boxplot of error values for the left ankle are shown in Figure 22.

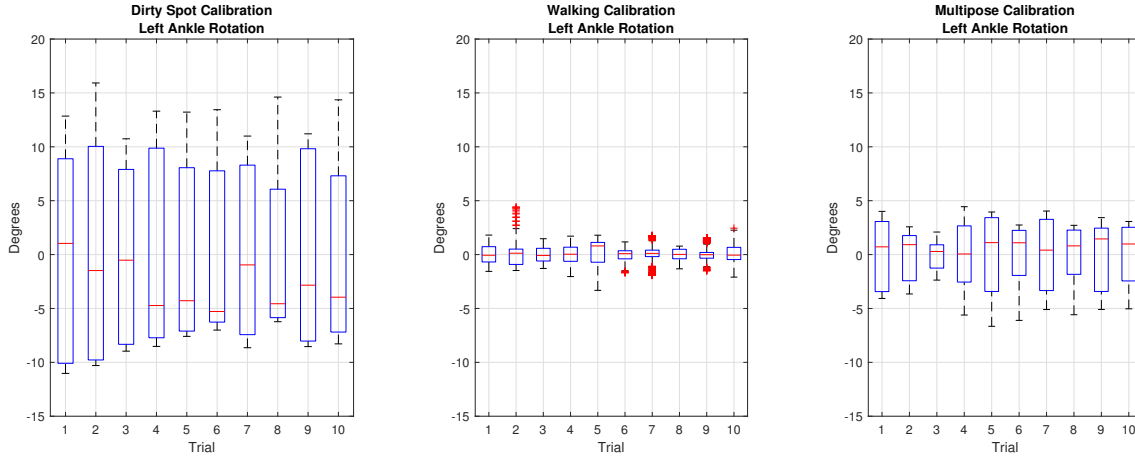


Figure 22: Dirty spot rotation error, left ankle
WC decreases the error of the dirty spot calibration and shows better results than the Multipose calibration.

Transversal Plane

The RMSE and ROM averaged over all trials are shown in Table 5.

Transversal Plane						
	Left Hip	Right Hip	Left Knee	Right Knee	Left Ankle	Right Ankle
RMSE (mean \pm std in $^{\circ}$)						
WC	$3,12 \pm 0,80$	$1,98 \pm 0,72$	$3,65 \pm 0,97$	$5,96 \pm 0,69$	$1,21 \pm 0,21$	$1,94 \pm 0,50$
MP	$2,19 \pm 1,10$	$2,39 \pm 0,83$	$3,95 \pm 1,47$	$7,68 \pm 0,78$	$1,16 \pm 0,17$	$1,73 \pm 0,55$
Restored	$2,81 \pm 0,44$	$1,29 \pm 0,52$	$2,51 \pm 0,58$	$12,8 \pm 0,82$	$1,30 \pm 0,41$	$1,59 \pm 0,41$
ROM (mean \pm std in $^{\circ}$)						
Reference	$7,95 \pm 1,30$	$10,0 \pm 1,56$	$12,2 \pm 1,82$	$15,2 \pm 1,65$	$3,02 \pm 0,99$	$3,98 \pm 0,81$
WC	$7,73 \pm 1,51$	$7,74 \pm 1,73$	$5,98 \pm 1,50$	$6,79 \pm 2,59$	$5,63 \pm 1,28$	$7,67 \pm 1,75$
MP	$7,04 \pm 1,22$	$8,12 \pm 1,90$	$6,27 \pm 2,69$	$9,24 \pm 2,72$	$5,09 \pm 1,61$	$7,18 \pm 2,04$
Restored	$6,70 \pm 1,05$	$9,08 \pm 1,65$	$13,3 \pm 3,16$	$21,1 \pm 1,67$	$6,35 \pm 1,22$	$7,26 \pm 2,09$

Table 5: Quantitative analysis of squats in dirty spot calibration trials, transversal plane
The mean and standard deviation was calculated over all 10 trials.

The RMSEs for movements in transversal were generally higher than for the coronal and sagittal plane with mean values up to 5.96° for WC and 7.68° for Multipose (both for right knee rotation). The functional calibration methods did not improve

the RMSE for the left hip and were higher than the static pose calibration for the right hip and left knee (Figure 23). The Range of Motion for Restored Metrics was closer to the ROM of the Reference for the mentioned angles as well.

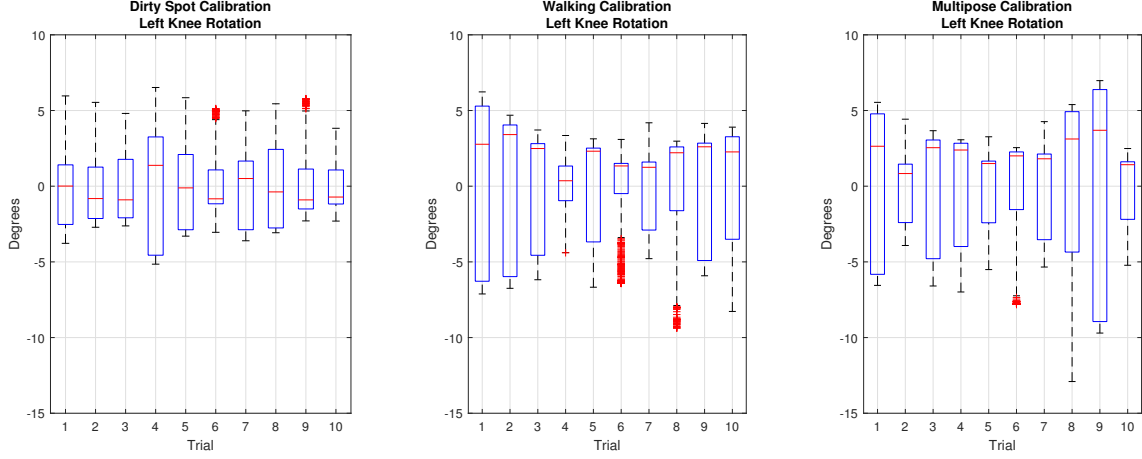


Figure 23: Dirty spot rotation error, left knee
The first and third quartile of WC and MP show a wider spread than the Restored Metrics.

For ankle abduction, all Calibration Methods showed similar results, as shown in ??.

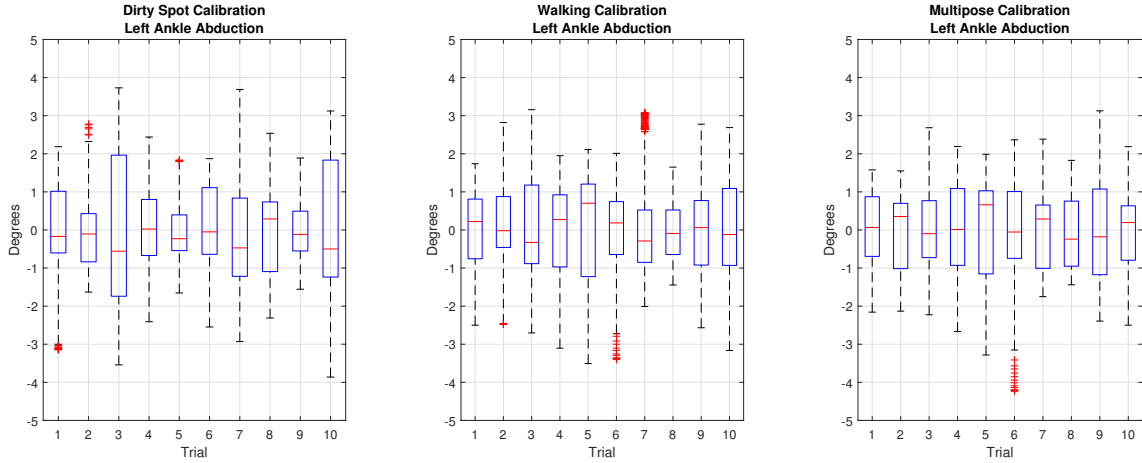


Figure 24: Dirty spot abduction error, left ankle

4.2 Clean Spot Calibration

4.2.1 Squats

Sagittal Plane

The average RMSE and ROM are shown in Table 6. The mean flexion RMSEs of the different calibration methods for the squats in clean initial calibration spot were all precise, with a maximum of 0.22° difference between the methods. An exception was the left ankle, with a difference of 0.70° between WC and MP. The absolute errors are all below 4° for all joints. The Range of Motion is similar between the IMU data. For the knee and ankle the ROM is between 3.4° - 7.0° lower than the Reference ROM.

Sagittal Plane						
	Left Hip	Right Hip	Left Knee	Right Knee	Left Ankle	Right Ankle
RMSE (mean \pm std in $^\circ$)						
WC	$1,82 \pm 0,32$	$1,55 \pm 0,20$	$2,19 \pm 0,16$	$2,46 \pm 0,24$	$2,68 \pm 0,31$	$2,29 \pm 0,25$
MP	$1,82 \pm 0,32$	$1,58 \pm 0,24$	$2,35 \pm 0,19$	$2,50 \pm 0,24$	$3,36 \pm 0,40$	$2,08 \pm 0,11$
Restored	$1,80 \pm 0,32$	$1,53 \pm 0,23$	$2,16 \pm 0,14$	$2,31 \pm 0,17$	$2,80 \pm 0,29$	$2,07 \pm 0,18$
ROM (mean \pm std in $^\circ$)						
Reference	$58,7 \pm 2,49$	$56,6 \pm 2,23$	$82,1 \pm 1,75$	$77,7 \pm 1,52$	$34,6 \pm 1,35$	$32,9 \pm 1,06$
WC	$61,2 \pm 2,98$	$56,4 \pm 3,13$	$77,0 \pm 1,72$	$72,5 \pm 1,76$	$29,2 \pm 1,17$	$28,9 \pm 1,50$
MP	$61,0 \pm 2,97$	$57,0 \pm 2,83$	$76,5 \pm 1,66$	$72,2 \pm 1,60$	$27,6 \pm 1,17$	$29,5 \pm 1,09$
Restored	$61,1 \pm 2,94$	$56,8 \pm 2,92$	$78,2 \pm 4,26$	$72,8 \pm 1,64$	$28,7 \pm 1,55$	$28,6 \pm 3,07$

Table 6: Quantitative analysis of squats in clean spot calibration trials, sagittal plane

The error boxplots for each calibration method showed similar distribution of errors for all methods. Exemplary, the right ankle plots are depicted in Figure 25.

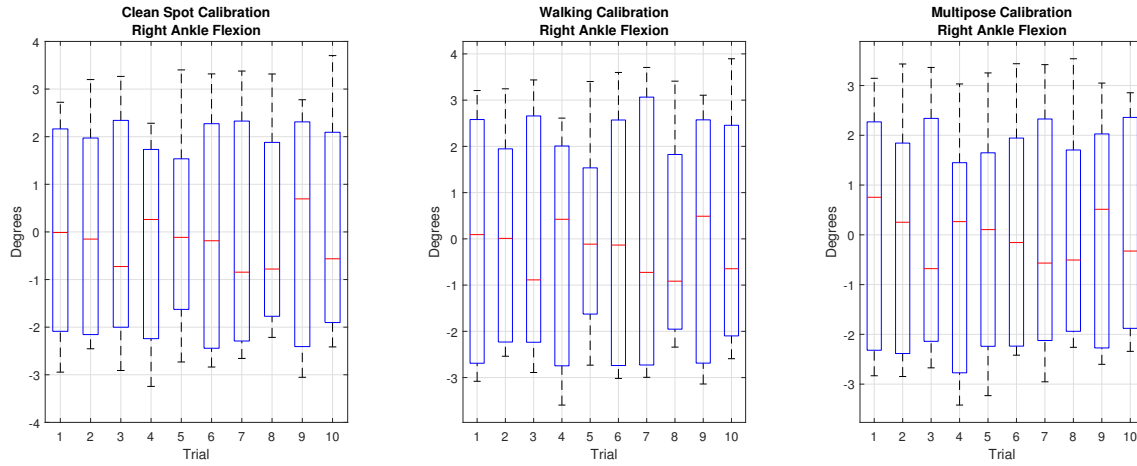


Figure 25: Clean spot dorsiflexion error, right ankle

Coronal Plane

Average RMSE and ROM for each calibration are shown in Table 7. Generally, the differences between the methods are higher than for flexion values. The most accurate method of each calibration was different for each joint and each body side. For the left knee, Multipose showed the lowest RMSE with 1.63° , yet it had the highest error for the right knee (4.07°). The box plots are shown in Figure 26. The ROM difference to the reference was highest with MP Calibration for all joints except the right hip.

Coronal Plane						
	Left Hip	Right Hip	Left Knee	Right Knee	Left Ankle	Right Ankle
RMSE (mean \pm std in $^\circ$)						
WC	$1,26 \pm 0,60$	$1,03 \pm 0,49$	$3,25 \pm 1,37$	$1,87 \pm 0,75$	$1,09 \pm 0,54$	$1,89 \pm 0,61$
MP	$2,22 \pm 0,89$	$1,04 \pm 0,42$	$1,63 \pm 0,95$	$4,07 \pm 1,38$	$4,35 \pm 0,75$	$4,33 \pm 0,95$
Restored	$1,11 \pm 0,25$	$1,26 \pm 0,44$	$4,39 \pm 1,47$	$2,84 \pm 0,77$	$0,99 \pm 0,33$	$2,48 \pm 0,44$
ROM (mean \pm std in $^\circ$)						
Reference	$3,66 \pm 0,60$	$6,75 \pm 1,40$	$8,64 \pm 1,10$	$4,26 \pm 0,58$	$5,54 \pm 1,52$	$5,04 \pm 1,61$
WC	$6,67 \pm 1,24$	$8,02 \pm 2,59$	$6,64 \pm 2,91$	$5,92 \pm 2,19$	$4,89 \pm 1,83$	$9,19 \pm 2,47$
MP	$7,77 \pm 1,32$	$6,01 \pm 0,72$	$11,4 \pm 3,47$	$11,0 \pm 3,49$	$11,0 \pm 2,87$	$14,8 \pm 3,22$
Restored	$5,88 \pm 1,19$	$5,39 \pm 1,42$	$6,19 \pm 1,55$	$7,96 \pm 2,18$	$4,86 \pm 1,22$	$10,5 \pm 2,28$

Table 7: Quantitative analysis of squats in clean spot calibration trials, coronal plane

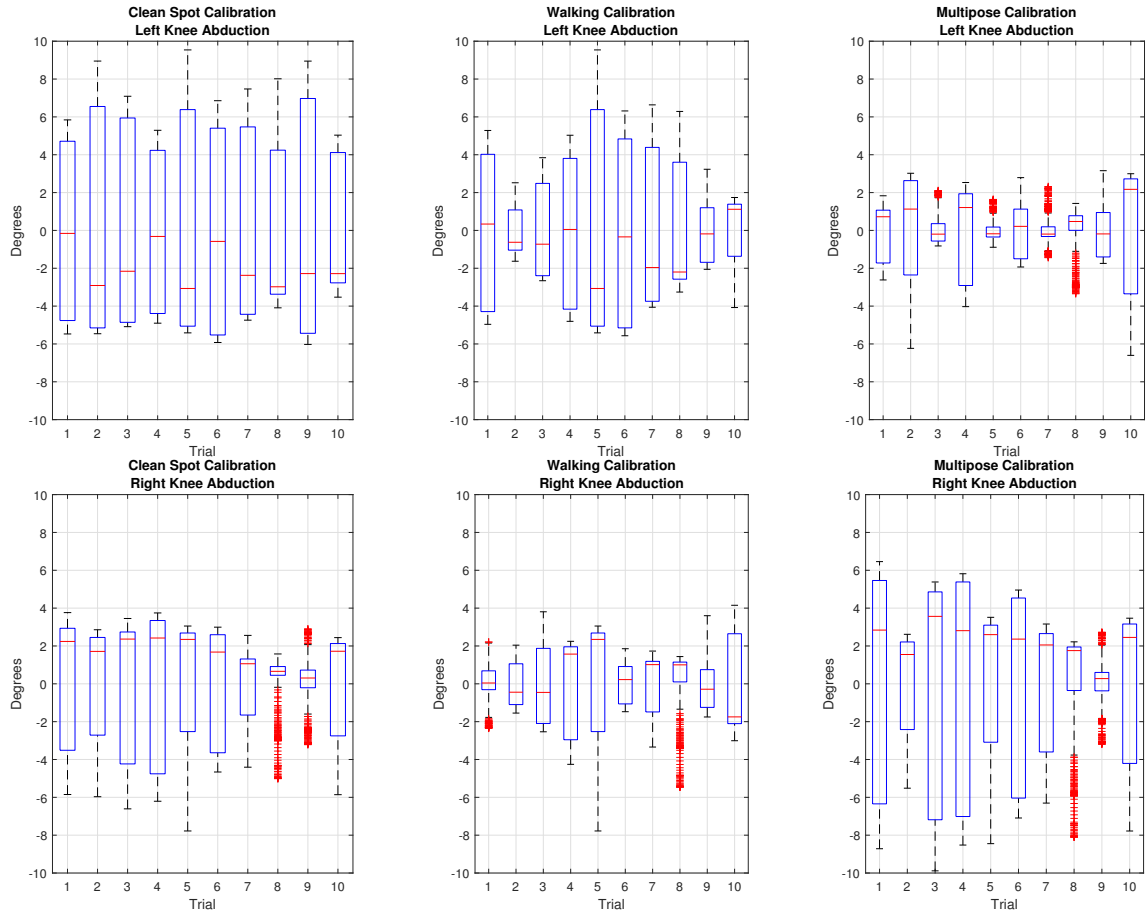


Figure 26: Clean spot abduction error, left and right knee
For the left knee, MP calibration shows the lowest difference to the reference,
whereas it is shows highest errors for the right knee.

RMSE for ankle inversion at both sides was higher for the MP calibration ($4.35^\circ/4.55^\circ$) than for the pose calibration ($0.99^\circ/2.48^\circ$) and WC($1.09^\circ/1.89^\circ$). Figure 27 showed the deployment of the error values for the left ankle.

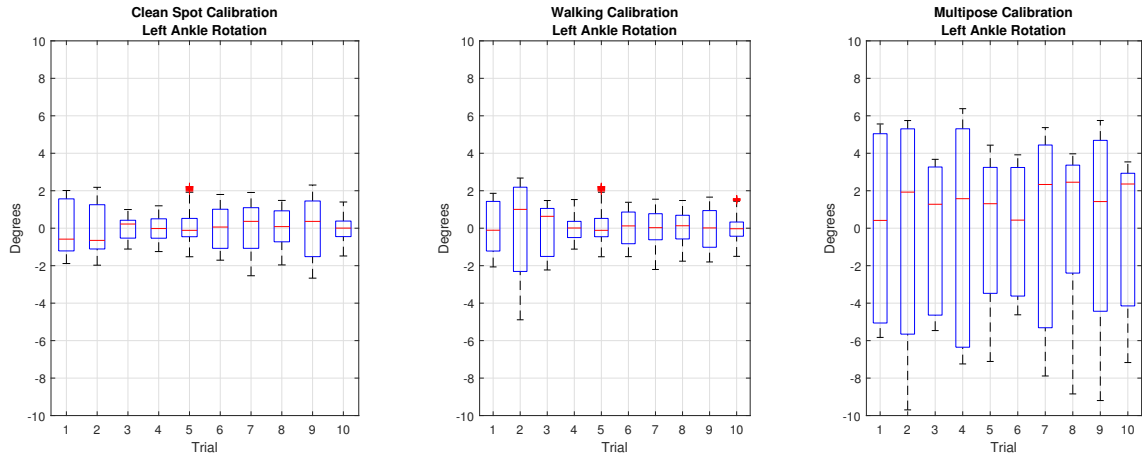


Figure 27: Clean spot inversion error, left ankle
Multipose Calibration error values are deployed wider and are not as precise as the pose calibration in clean spot and Walking Calibration.

Transversal Plane

Average RMSE and ROM for each calibration are shown in Table 8. Differences for the RMSEs of the hip joints went up to 1.51° (Restored-MP, Left Hip).

Transversal Plane						
	Left Hip	Right Hip	Left Knee	Right Knee	Left Ankle	Right Ankle
RMSE (mean \pm std in $^\circ$)						
WC	$2,67 \pm 0,63$	$2,36 \pm 0,79$	$3,61 \pm 0,97$	$5,71 \pm 0,96$	$1,62 \pm 0,79$	$2,29 \pm 0,41$
MP	$1,27 \pm 0,43$	$2,53 \pm 0,56$	$4,73 \pm 1,11$	$7,96 \pm 1,12$	$1,73 \pm 0,83$	$1,86 \pm 0,32$
Restored	$2,78 \pm 0,23$	$1,83 \pm 0,47$	$3,30 \pm 2,60$	$7,60 \pm 0,68$	$1,68 \pm 0,67$	$2,11 \pm 0,38$
ROM (mean \pm std in $^\circ$)						
Reference	$7,80 \pm 1,11$	$11,5 \pm 0,95$	$12,3 \pm 1,55$	$14,4 \pm 0,80$	$2,80 \pm 1,02$	$3,37 \pm 0,55$
WC	$6,48 \pm 2,18$	$8,93 \pm 1,90$	$6,87 \pm 2,49$	$6,75 \pm 2,07$	$5,74 \pm 1,61$	$8,50 \pm 1,63$
MP	$5,96 \pm 1,42$	$8,83 \pm 2,43$	$7,87 \pm 2,07$	$10,7 \pm 2,70$	$6,03 \pm 2,26$	$7,54 \pm 1,73$
Restored	$6,05 \pm 1,90$	$9,32 \pm 2,46$	$6,39 \pm 2,49$	$9,91 \pm 1,67$	$5,49 \pm 1,37$	$8,13 \pm 1,77$

Table 8: Quantitative analysis of squats in clean spot calibration trials, transversal plane

Generally, knee rotation showed high RMSE values up to 7.96° . It was smallest for the Walking Calibration, but with only small deviations between the different IMU calibration methods (Figure 28).

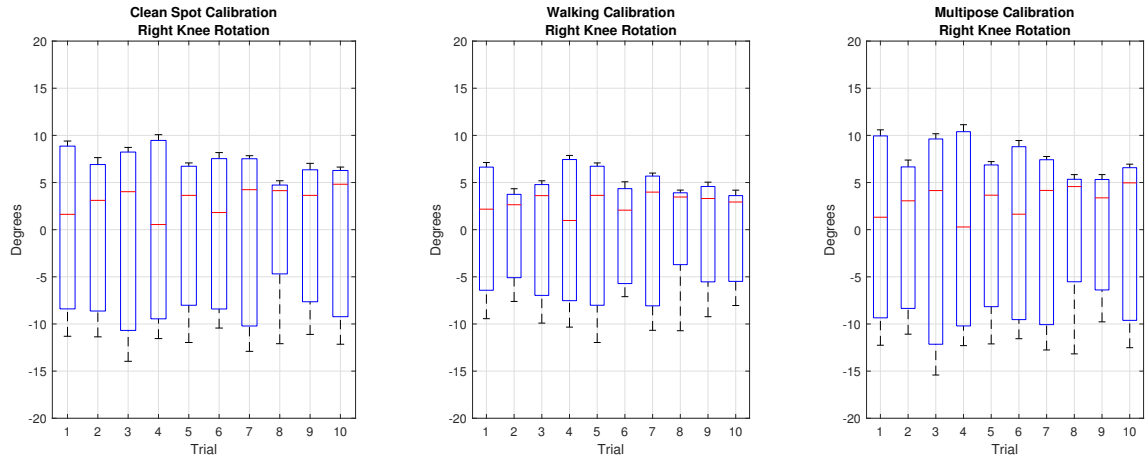


Figure 28: Clean spot rotation error, right knee

For the ankle abduction, no significant differences between the IMU methods could be detected. Trial 9 showed a higher error deployment range than the other trials as shown in Figure 29.

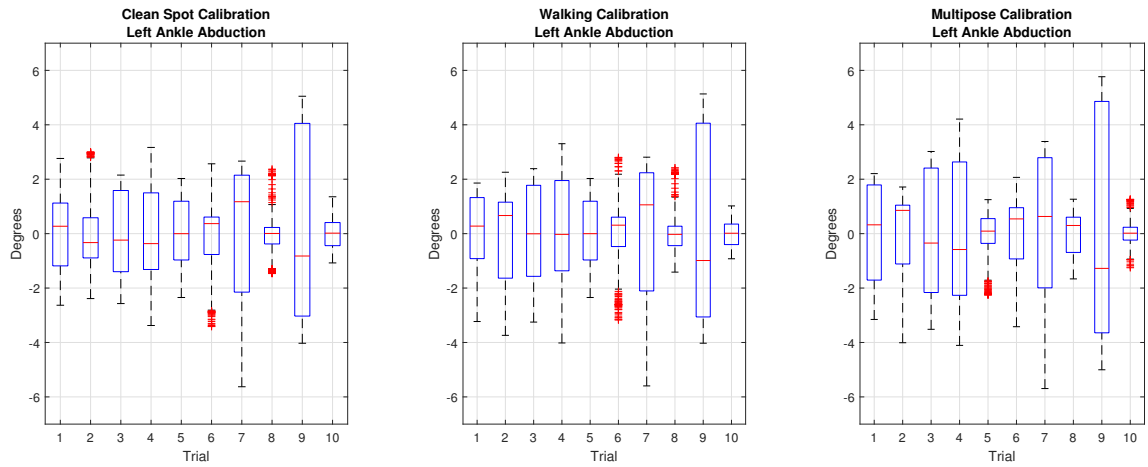


Figure 29: Clean spot abduction error, left ankle

5 Discussion

5.1 General Annotations

The aim of this study was to validate two new Functional Calibration methods, "Walking Calibration" and "Multipose", for the Noraxon MyoMotion Inertial Measurement System. With an initial calibration in an assumed magnetically inhomogeneous spot, the system was used in a place where the manufacturer usually does not recommend using the system. The Functional Calibration methods represent a supplement to the normal static pose calibration, meant to increase the usability of the IMU system for users which can not provide a magnetically homogeneous spot. The male subject which was examined performed the Functional Calibration Methods without help of another operator. All trials could be recorded and processed in the first attempt. Movement of all lower limb joints were compared to an optical reference system for gait and squat movements.

In order to qualitatively analyse the data, constant offsets to the reference were removed by subtraction. The offset between the measurements were different for each trial, which is related to the quality of the initial calibration, but also the quality of the Multipose calibration. The different offsets can be found in the appendix. Generally, the differences of offsets between IMU data are higher for the calibration in the dirty spot than for the trials in the clean spot. This finding is important for the consideration of absolute values. In this study, the focus of observation was put more on qualitative movement analysis. When considering Ranges of Motion, the offsets do not play a role as well.

Gait Analysis

Since the gait cycles could not be normalized due to insufficient data, the steps had to be plotted over time after the respective heel strike. In biomechanics, the steps are usually normalized and plotted via the percentage of the gait cycle. Based on the available data, the x-axis and therefore the limit of each step was set to 125 seconds. When comparing the findings of this study with present literature, the analyzed time stamp was therefore divided by 125s to compare it with other studies.

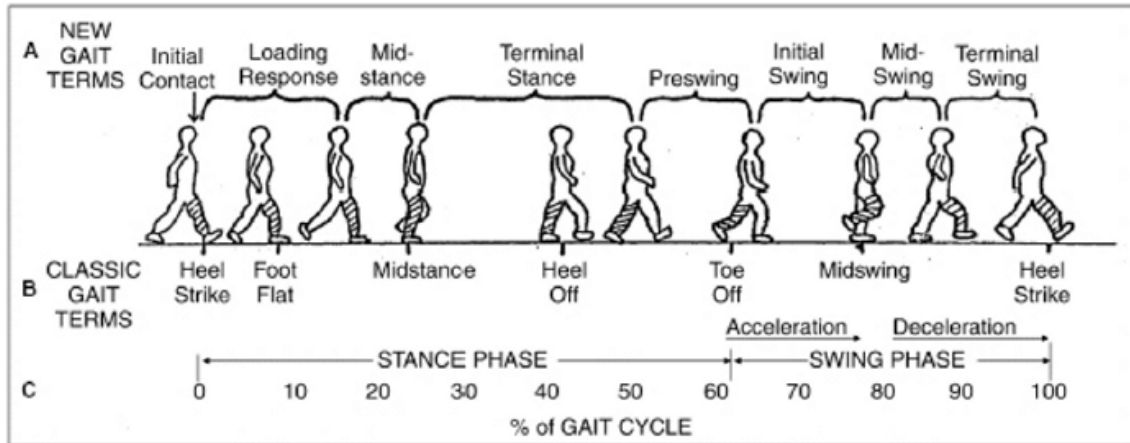


Figure 30: Phases of the gait cycle (Castermans et al. 2013)

Beginning of the swing phase at 60 % of the gait cycle matches with approximately 75 seconds after the heel strike in this study.

Deviations in kinematic measurements

In clinical use of kinematic motion analysis, the main focus is on the deviation from norm values in motion patterns. However, due to variability of the measurement results, there is no fixed minimal clinical important difference (MCID) for joint angles. In fact, previous studies showed minimal detectable changes (MDC) of greater than 5° identified in different sessions for the same subject with no change of pathologic condition (Wilken et al. 2012). Furthermore, the Noraxon MyoMotion System has an anatomical angle accuracy of $\pm 2^\circ$ in dynamic conditions, according to the manufacturer. On top of the mentioned factors, it has to be taken into account that both of the used measurements are prone to soft tissue artefacts. Muscle contraction causes movement of the skin, which can falsely indicate movement of the body segment. This applies to marker based systems same as the IMU system (Cloete and Scheffer 2010). In this study, the limit for an acceptable error was therefore set to 5° by the author.

5.2 Dirty Spot Calibration

Movements in Sagittal Plane

The findings for flexion movements show the most accurate results for all joints in gait and squats. The gait cycles of the hip joints are congruent for all IMU methods and show minor deviations to the reference. For the knees, maximal Multipose and Walking Calibration are significantly closer to the maximal reference knee flexion in the mid swing phase. Also, the ROM of the curves is closer to the reference. Compared to the reference, restored metrics show a higher dorsiflexion in the beginning of the stance phase, but a higher plantar flexion in the swing phase, both of which was corrected by the Functional Calibration methods. All of the flexion curves match with results of other studies (Ferrari et al. 2008; Gao and Zheng 2010). Those findings match with the results of the squat trials. Here, the ROM of Knee and Ankle are closer to the Reference and the boxplots show, that the error of flexion could be reduced to lower values than $\pm 5^\circ$ for both knees and both ankles. In Trial 5 Multipose produced completely wrong results as shown in Figure 19. Because this error only occurred with the left ankle, it is probably caused either by an incorrect posture in the Multipose posture or while processing the data. Other than this outlier, the data was very reliable, with standard deviations for the RMSE values lower than 0.5° for both Functional calibration methods. The results are equally good as findings in other IMU studies (Seel, Raisch, and Schauer 2014).

Movements in Coronal Plane

The most obvious improvement of the dirty spot calibration data can be found for the knee abduction. Here, the wrongly assumed orientation of the sensors cause anomalously high abduction during gait (Figure 15). The corrected curves are closer to the curve of the reference system and also match with findings in the previously mentioned research papers.

Clear improvements can as well be found for the inversion of ankles within the Walking Calibration data. Here, the gait cycle follows the reference and match other studies for both ankles (Ferrari et al. 2008). For the Multipose calibration, this is only the case for the left ankle as shown in Figure 16. For the right ankle,

Multipose indicates a much higher external rotation at the beginning of the swing phase. For Abduction of the Hip, the quality of the Functional Calibration curves increase the data in the beginning of the swing phase. The squat analysis matches the results, improving the heavily spoiled knee abduction. Yet, the RMSE for the knee abduction stayed relatively high. The ROM of the IMU data is twice as high. The hip abduction error could also be reduced by Multipose and Walking Calibration. Correction of Ankle Rotations seems to work accurately, with Walking Calibration being superior to Multipose (Figure 27)

Movements in Transversal Plane

For the ankle Abduction presented in Figure 15, the deflection of the curves are of unknown origin. For the right ankle, the same deflection is detected, for this side it indicates adduction for all methods. The deflection happens at the same time than the ones in the coronal plane. It is possibly caused by movement of the sensor while lifting the foot. To exclude the possibility of such errors, it is usually recommended to wear inertial measurement units tied to a shoe, which was not possible in this study because the optical markers had to be placed on the anatomical landmarks of the foot. Absolute errors stay in an acceptable range for the rest of the cycle, as the Range of Motion is quite small. The Curves for rotation of the hip were similar for each calibration method of the IMU system. The curves deviated to the reference in the swing phase. For knee rotation, the gait curves once again showed deviations at the beginning of the swing phase. This deflection was bigger for Multipose than for the Walking Calibration and does not match with findings in the literature (Cloete and Scheffer 2010). The results of qualitative gait analysis matches with the squat trials. Ankle abduction shows low RMSE values, but it has to be taken into account that the Range of Motion is relatively low for the squat movement. For the IMU data, the Range of Motion indicated a rotation of up to 7° , while the reference indicated up to 4° .

Knee rotation showed high RMSE values of 3.65° - 7.68° for the functional calibration methods. Considering a range of motion of only 12.2° - 15.2° this error is remarkably high. The functional calibration methods also did not improve the hip rotation, with RMSE values up to 2.47° for gait and 3.12° for squat movements. This is relatively high compared to the small range of motion.

5.3 Clean Spot Calibration

The differences between the Functional Calibration methods and the standard pose calibration are not significant for all flexion angles. Here too, the constant offset between each calibration method was smaller than 2° for all angles. For the abduction angles, there is no clear tendency for a most accurate calibration method, because for each angle a different method gave the smallest error. However, the calibration methods did not deteriorate the restored clean calibration metrics, just for the right knee abduction the RMSE was higher for the Multipose Calibration. For the abduction, very different offsets for the ankle abduction were noticed. The mean offset was 7° for the left ankle compared to close to 0° for WC and Clean Calibration Metrics. For the left ankle, the Walking Calibration produced a mean offset of 14.19° compared to ca. 4.50° for the other methods. For the analysis of rotation angles, Multipose calibration shows the worst results of all methods. The method seems to deteriorate the Restored Metrics. The Range of Motion of the left ankle is more than twice as big as the ones of the other methods. The error values for the Walking calibration are not significantly higher or lower than the ones of clean spot calibration data. The mean rotation offset to the reference was also higher for the Multipose than it was for the other methods, with a difference up to 5.70° (left ankle, 7.356° for MP, 1.656° for clean spot calibration). The results for the right knee rotation are inaccurate for all methods. The restored metrics also show a difference in the offset of almost 10° to Walking Calibration. If you look at the absolute values, this would mean even higher RMSE values, if the offset would not be corrected. For the use of the same system, with the same alignment of sensors, this does not indicate reliable data.

5.4 Summary

In the present study, the focus was on the basic functionality of the Functional Calibration Methods Walking Calibration and Multipose. The aim was to demonstrate the possibility of using the MyoMotion IMU system without the necessary condition of a magnetically homogeneous calibration spot. Basically, an improvement of the usability of the wearable IMU sensor system MyoMotion could be proven with the qualitative analysis of gait cycles and the evaluation of errors compared to a

reference. The qualitative analysis shows that course orientation errors of the static pose calibration in a magnetically disturbed place lead to spoiled data in almost all joint movements examined. Walking Calibration and Multipose are suitable tools to correct this orientation error.

For flexion values of the lower limb, the improvements can be determined both qualitatively and quantitatively. The results are equally good as findings in other IMU studies (Seel, Raisch, and Schauer 2014; Picerno, Cereatti, and Cappozzo 2008). In the coronal plane, the data was spoiled most significantly and could be corrected for all joints. Deviations in the gait curves were observed mostly in the swing phase. For movements in the transversal plane, the reliability of the methods could not be confirmed for all joint angles. Especially the knee joint shows big deviations. Other functional calibration methods suggest to take advantage of the anatomical knowledge and consider the knee as a hinge joint (Cooper et al. 2009; Lee and Jeon 2018). This would significantly simplify the kinematic analysis of this joint. Other functional calibration approaches also showed moderate accuracy for the knee joint (Favre et al. 2009). There is less information in the literature for evaluating rotational movements of the joints than, for example movements, in the sagittal plane. For IMU technology in particular, the measurement of these movements, which have smaller ranges of motion in gait and squat, is generally less reliable (Poitras et al. 2019; Picerno, Cereatti, and Cappozzo 2008). This suggests that the high transversal plane errors in this study were caused by limitations of the IMU technology in general rather than by the functional calibration methods. The fact, that the RMSE of the clean spot calibration was also higher for rotation/foot abduction than for knee and hip abduction/flexion, also speaks for that. Nevertheless, especially the correct course orientations are decisive for the rotation of joints.

The Functional calibration methods also does not seem to deteriorate the clean spot pose calibration, which is an important criteria for the validity of the methods. However, the RMSE analysis has to be cautiously reviewed, as the constant offset between the methods varied in an unacceptable range.

From the data acquired in this study, Walking Calibration seems to be the superior method over Multipose. It is also less susceptible to false executions, if a straight gait can be guaranteed for example by markings on the floor. In the MR3 software,

wrong executions are also detected right after the procedure, which happened multiple times in a different setting before the day of measurement. However, one must consider that the laboratory or motion clinic must have space for a patient to walk at least 5m to perform the Walking Calibration. In small rooms, the Multipose Procedure is much easier to implement. The data for this calibration also showed improvement, but seemed to spoil the clean calibration data. This could be due to an error in the measurement setup, as explained in the next section. Multipose calibration requires a good execution of movement and might be more difficult to implement for patients with physical disabilities or for elderly people.

5.5 Limitations and suggestions for future research

In the present study, several limitations and sources of errors have to be considered. As previously mentioned, a standardization of gait, as is common in biomechanics, could not be carried out due to the measurement setup. This also influences the evaluation of data, since the gait speed might vary between the trials and lead to averaging different phases of the gait cycle. As there was just one subject who performed all trials after each other, this source of error can be considered low.

Another possible source of errors lies within the measurement setup itself. As mentioned in the description of the Functional Calibration methods, wrong execution of the procedures were accepted in this study. With the aim to compare the two methods in the same measurement, the Multipose calibration was carried out after the walking calibration. In the meantime, the sensors could suffer from drift. This would mean, that the movement in the sagittal plane as explained in subsubsection 2.6.2, could be affected not only by wrong execution but by the assumed sensor orientation itself.

Furthermore, it has been shown that different anatomic models lead to variations in kinematic analysis of angles (Mundt et al. 2019). The anatomical model of the Qualisys system differs to the one which is used by Noraxon. With equal models, the understanding of differences in the data should be better.

With only one male subject, the study had more of an exploratory character. There was no variation of physical constitution and the IMU sensors were fixated to the body segments in the exact way. Different fixation of the sensors might lead

to other results. The subject had previously executed the calibration procedures. Inexperienced subjects might have a higher susceptibility to incorrect execution of the calibration movements, which could decrease the functionality of the methods in applied biomechanical investigations.

Further evaluations of the Calibration Methods should focus on movements in transversal plane, as results of this study require further consideration. Examinations of more subjects would make systematic validation with more statistical parameters possible. To reduce the possibility of drift errors, the Functional Calibration methods should, as intended, both be executed immediately after the initial calibration. If both methods are measured in one trial, this could be done by another pose calibration before the Multipose.

Another issue worth investigating are the differences of offsets for each calibration method. In this study, the mean errors were eliminated in order to compare the different IMU models to the reference. Differences between IMU data, especially for the clean calibration data, are however undesirable and should be addressed in a study. With the Noraxon MyoMotion system, the orientation angles can be evaluated for each sensor. The data that was recorded for this study could thusly also be investigated further, with focus on the course orientation of each sensor for the different methods.

6 Conclusion

The hypotheses of the study can mostly be affirmed. The quality and accuracy of joint kinematics was increased by the Functional Calibration methods for most of the lower limb joint movements. Both approaches, Walking Calibration and Multipose, show similar results with slightly better results for Walking Calibration. In clinics or movement laboratories where no calibration spot with magnetic homogeneity can be found, the methods increase the usability of the MyoMotion system.

Movements in the transversal plane have to be reviewed. The deviations were higher here, but this also applied to the clean spot calibration. Thus it should be further examined whether there is a calibration method that can give the most reliable results for movements in the transversal plane.

In magnetically homogeneous spots, the differences of RMSE values are in acceptable range. Multipose Calibration showed worse results for some joints, but was subject to an error-prone measurement setup. If a magnetically homogeneous calibration spot can be guaranteed, the normal pose calibration should nevertheless be carried out, since the offsets between the calibration methods fluctuated more than expected and therefore still require further investigation.

References

- Borenstein, Johann, Lauro Ojeda, and Surat Kwanmuang (2009). “Heuristic reduction of gyro drift in IMU-based personnel tracking systems”. In: *Optics and Photonics in Global Homeland Security V and Biometric Technology for Human Identification VI*. Vol. 7306. International Society for Optics and Photonics, 73061H.
- Bouza, Juan Pablo (n.d.). *Body Planes*. [Online; 07/05/2020]. URL: https://commons.wikimedia.org/wiki/File:Human_anatomy_planes.svg.
- Cappozzo, Aurelio et al. (1995). “Position and orientation in space of bones during movement: anatomical frame definition and determination”. In: *Clinical biomechanics* 10.4, pp. 171–178.
- Castermans, Thierry et al. (Mar. 2013). “Towards Effective Non-Invasive Brain-Computer Interfaces Dedicated to Gait Rehabilitation Systems”. In: *Brain Sciences* 4, pp. 1–48. DOI: [10.3390/brainsci4010001](https://doi.org/10.3390/brainsci4010001).
- Cloete, Teunis and Cornie Scheffer (2010). “Repeatability of an off-the-shelf, full body inertial motion capture system during clinical gait analysis”. In: *2010 Annual International Conference of the IEEE Engineering in Medicine and Biology*. IEEE, pp. 5125–5128.
- Cockroft, Stephen John (2015). “Novel motion capture methods for sports analysis: case studies of cycling and rugby goal kicking”. PhD thesis. Stellenbosch: Stellenbosch University.
- Cooper, Glen et al. (2009). “Inertial sensor-based knee flexion/extension angle estimation”. In: *Journal of biomechanics* 42.16, pp. 2678–2685.
- De Vries, WHK et al. (2008). “Magnetic distortion in motion labs, implications for validating inertial magnetic sensors”. In: *Gait & posture* 29.4, pp. 535–541.

- Favre, Julien et al. (2009). “Functional calibration procedure for 3D knee joint angle description using inertial sensors”. In: *Journal of biomechanics* 42.14, pp. 2330–2335.
- Ferdinando, Hany, Handry Khoswanto, and Djoko Purwanto (2012). “Embedded Kalman filter for inertial measurement unit (IMU) on the ATmega8535”. In: *2012 International Symposium on Innovations in Intelligent Systems and Applications*. IEEE, pp. 1–5.
- Ferrari, Alberto et al. (2008). “Quantitative comparison of five current protocols in gait analysis”. In: *Gait & posture* 28.2, pp. 207–216.
- Galarnyk, Michael (2018). *Understanding Boxplots*. Online, 07/05/2020. URL: https://commons.wikimedia.org/wiki/File:Human_anatomy_planes.svg.
- Gao, Bo and Naiquan Nigel Zheng (2010). “Alterations in three-dimensional joint kinematics of anterior cruciate ligament-deficient and-reconstructed knees during walking”. In: *Clinical biomechanics* 25.3, pp. 222–229.
- Iosa, Marco et al. (2016). “Wearable inertial sensors for human movement analysis”. In: *Expert Review of Medical Devices* 13.7. PMID: 27309490, pp. 641–659. DOI: [10.1080/17434440.2016.1198694](https://doi.org/10.1080/17434440.2016.1198694). URL: <https://doi.org/10.1080/17434440.2016.1198694>.
- Kainz, Hans et al. (2016). “Joint kinematic calculation based on clinical direct kinematic versus inverse kinematic gait models”. In: *Journal of biomechanics* 49.9, pp. 1658–1669.
- Kardos, Slavomir, Peter Balog, and Stanislav Slosarcik (2017). “Gait dynamics sensing using IMU sensor array system”. In: *Advances in Electrical and Electronic Engineering* 15.1, pp. 71–76.

- Kruk, Eline van der and Marco M Reijne (2018). “Accuracy of human motion capture systems for sport applications; state-of-the-art review”. In: *European journal of sport science* 18.6, pp. 806–819.
- Laidig, Daniel, Philipp Müller, and Thomas Seel (2017). “Automatic anatomical calibration for IMU-based elbow angle measurement in disturbed magnetic fields”. In: *Current directions in biomedical engineering* 3.2, pp. 167–170.
- Laidig, Daniel, Thomas Schauer, and Thomas Seel (2017). “Exploiting kinematic constraints to compensate magnetic disturbances when calculating joint angles of approximate hinge joints from orientation estimates of inertial sensors”. In: *2017 International Conference on Rehabilitation Robotics (ICORR)*. IEEE, pp. 971–976.
- Lee, Jung Keun and Mi Jin Choi (2019). “Robust inertial measurement unit-based attitude determination Kalman filter for kinematically constrained links”. In: *Sensors* 19.4, p. 768.
- Lee, Jung Keun and Tae Hyeong Jeon (2018). “IMU-based but magnetometer-free joint angle estimation of constrained links”. In: pp. 1–4.
- Luinge, Henk J, Peter H Veltink, and Chris TM Baten (2007). “Ambulatory measurement of arm orientation”. In: *Journal of biomechanics* 40.1, pp. 78–85.
- Michaelson, Tobias (2018). “Lagebestimmung durch Sensorfusion mittels Kalmanfilter”. In: *Masterarbeit*.
- Morton, Lee, Lynne Baillie, and Roberto Ramirez-Iniguez (2013). “Pose calibrations for inertial sensors in rehabilitation applications”. In: *2013 IEEE 9th International Conference on Wireless and Mobile Computing, Networking and Communications (WiMob)*. IEEE, pp. 204–211.

- Mundt, Marion et al. (2019). “Assessment of the measurement accuracy of inertial sensors during different tasks of daily living”. In: *Journal of biomechanics* 84, pp. 81–86.
- Nowicki, Michal and Roman Szewczyk (2015). “Modeling of Earth Magnetic Field Disturbances Induced by Ferromagnetic Objects”. In:
- Oberlaender, Dr. rer. nat. Kai (2015). *Inertial Measurement Uni (IMU) Technology*.
- Palermo, Eduardo et al. (2014). “Experimental evaluation of accuracy and repeatability of a novel body-to-sensor calibration procedure for inertial sensor-based gait analysis”. In: *Measurement* 52, pp. 145–155.
- Picerno, Pietro, Andrea Cereatti, and Aurelio Cappozzo (2008). “Joint kinematics estimate using wearable inertial and magnetic sensing modules”. In: *Gait & posture* 28.4, pp. 588–595.
- Poitras, Isabelle et al. (2019). “Validity and reliability of wearable sensors for joint angle estimation: A systematic review”. In: *Sensors* 19.7, p. 1555.
- Seel, Thomas, Jörg Raisch, and Thomas Schauer (2014). “IMU-based joint angle measurement for gait analysis”. In: *Sensors* 14.4, pp. 6891–6909.
- Shull, Pete B et al. (2014). “Quantified self and human movement: a review on the clinical impact of wearable sensing and feedback for gait analysis and intervention”. In: *Gait & posture* 40.1, pp. 11–19.
- TeachMeAnatomy (2015). *Anatomical Terms of Movement*. URL: <https://teachmeanatomy.info/the-basics/anatomical-terminology/terms-of-movement/>.
- Vargas-Valencia, Laura Susana et al. (2016). “An IMU-to-body alignment method applied to human gait analysis”. In: *Sensors* 16.12, p. 2090.

- Wilken, Jason M et al. (2012). “Reliability and minimal detectible change values for gait kinematics and kinetics in healthy adults”. In: *Gait & posture* 35.2, pp. 301–307.
- Wong, Wai Yin, Man Sang Wong, and Kam Ho Lo (2007). “Clinical Applications of Sensors for Human Posture and Movement Analysis: A Review”. In: *Prosthetics and Orthotics International* 31.1. PMID: 17365886, pp. 62–75. DOI: [10.1080/03093640600983949](https://doi.org/10.1080/03093640600983949). URL: <https://doi.org/10.1080/03093640600983949>.
- Wu, Ge and Peter R Cavanagh (1995). “ISB recommendations for standardization in the reporting of kinematic data”. In: *Journal of biomechanics* 28.10, pp. 1257–1261.
- Zeni Jr, JA, JG Richards, and JS Higginson (2008). “Two simple methods for determining gait events during treadmill and overground walking using kinematic data”. In: *Gait & posture* 27.4, pp. 710–714.

A Gait Plots

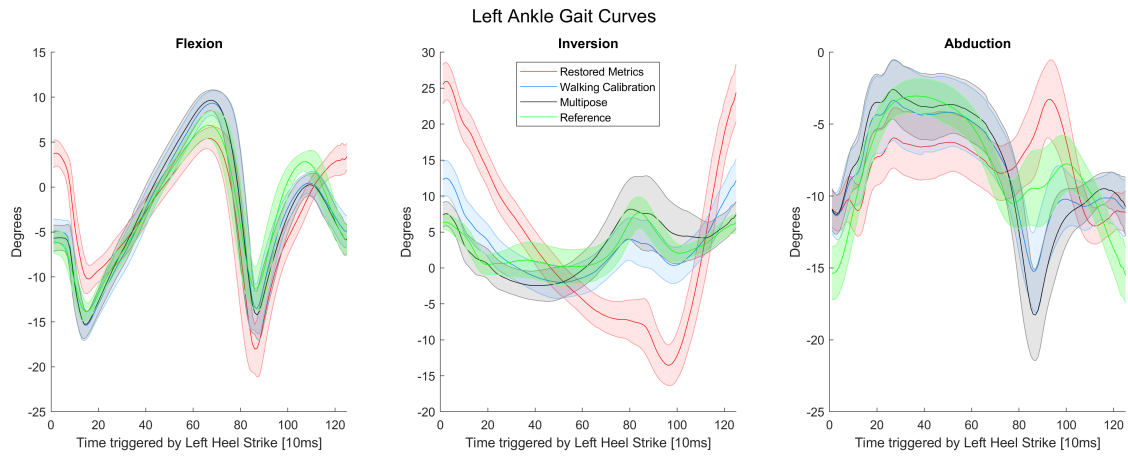


Figure 31: Left Ankle Gait Curves

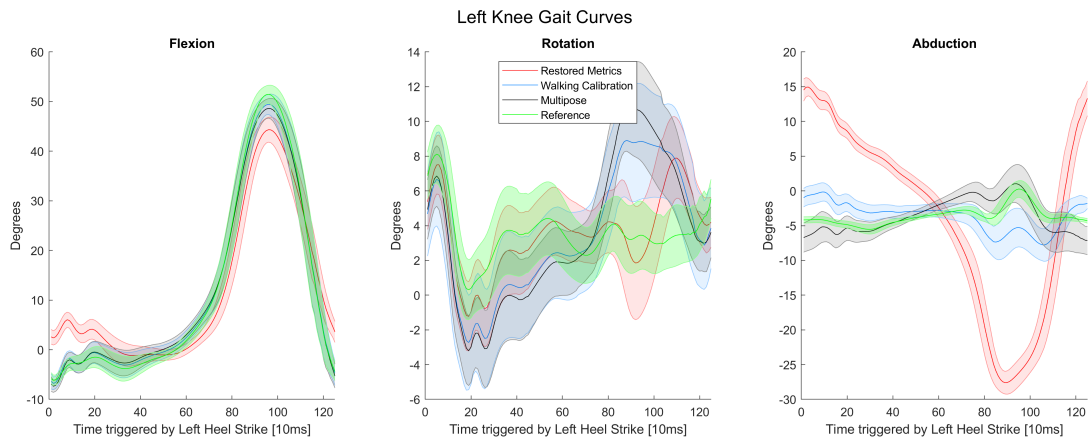


Figure 32: Left Knee Gait Curves

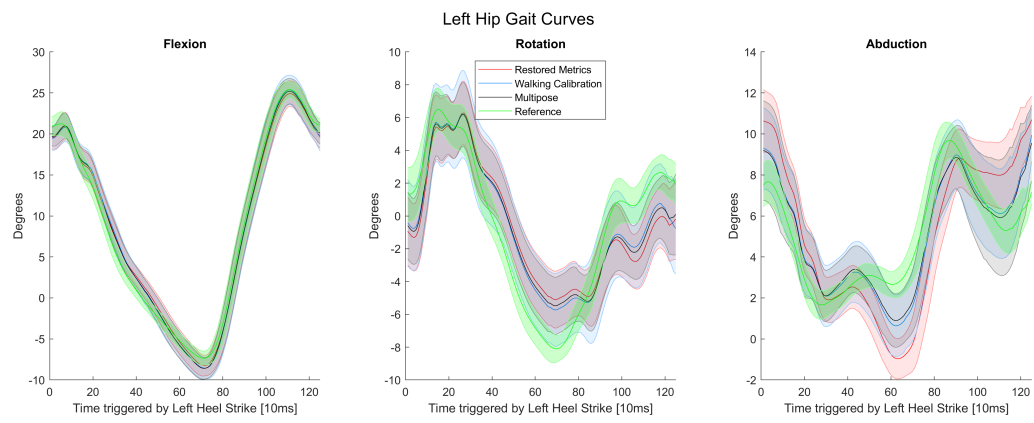


Figure 33: Left Hip Gait Curves

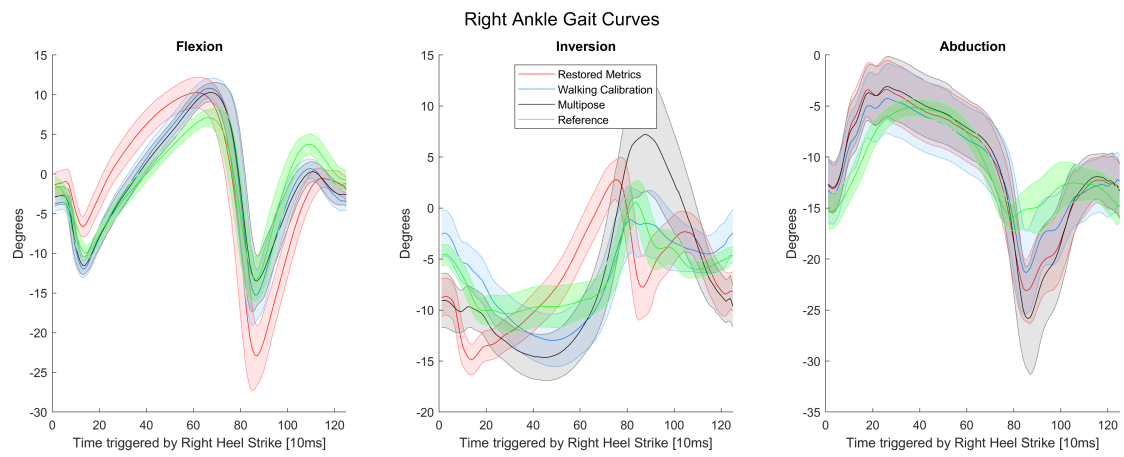


Figure 34: Right Ankle Gait Curves

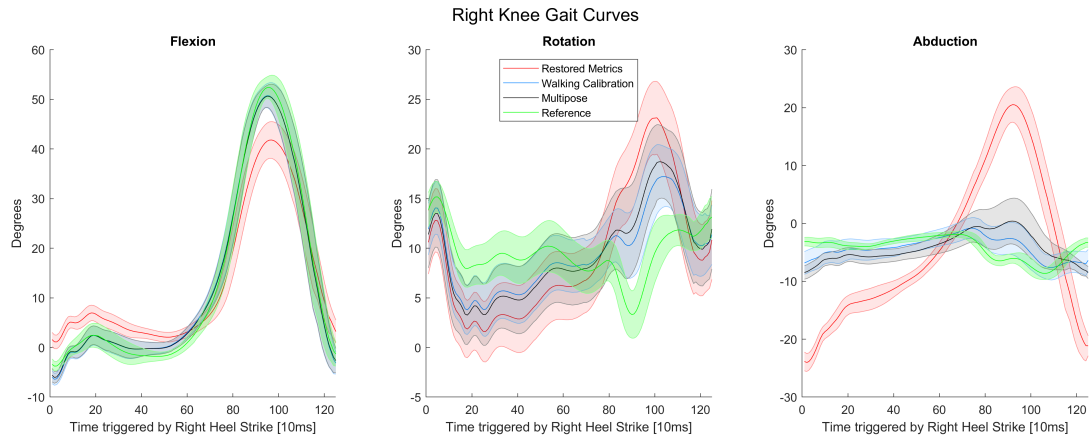


Figure 35: Right Knee Gait Curves

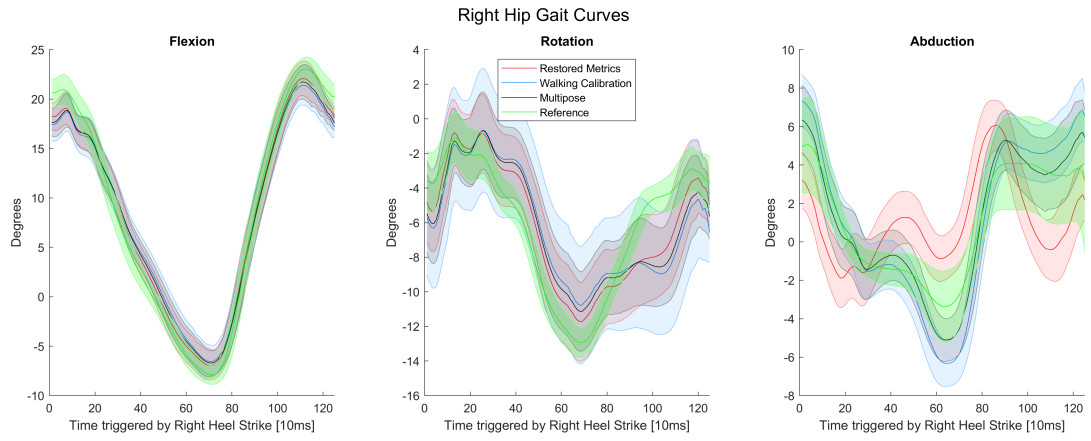


Figure 36: Right Hip Gait Curves

B Squat Plots

B.1 Dirty Spot Calibration

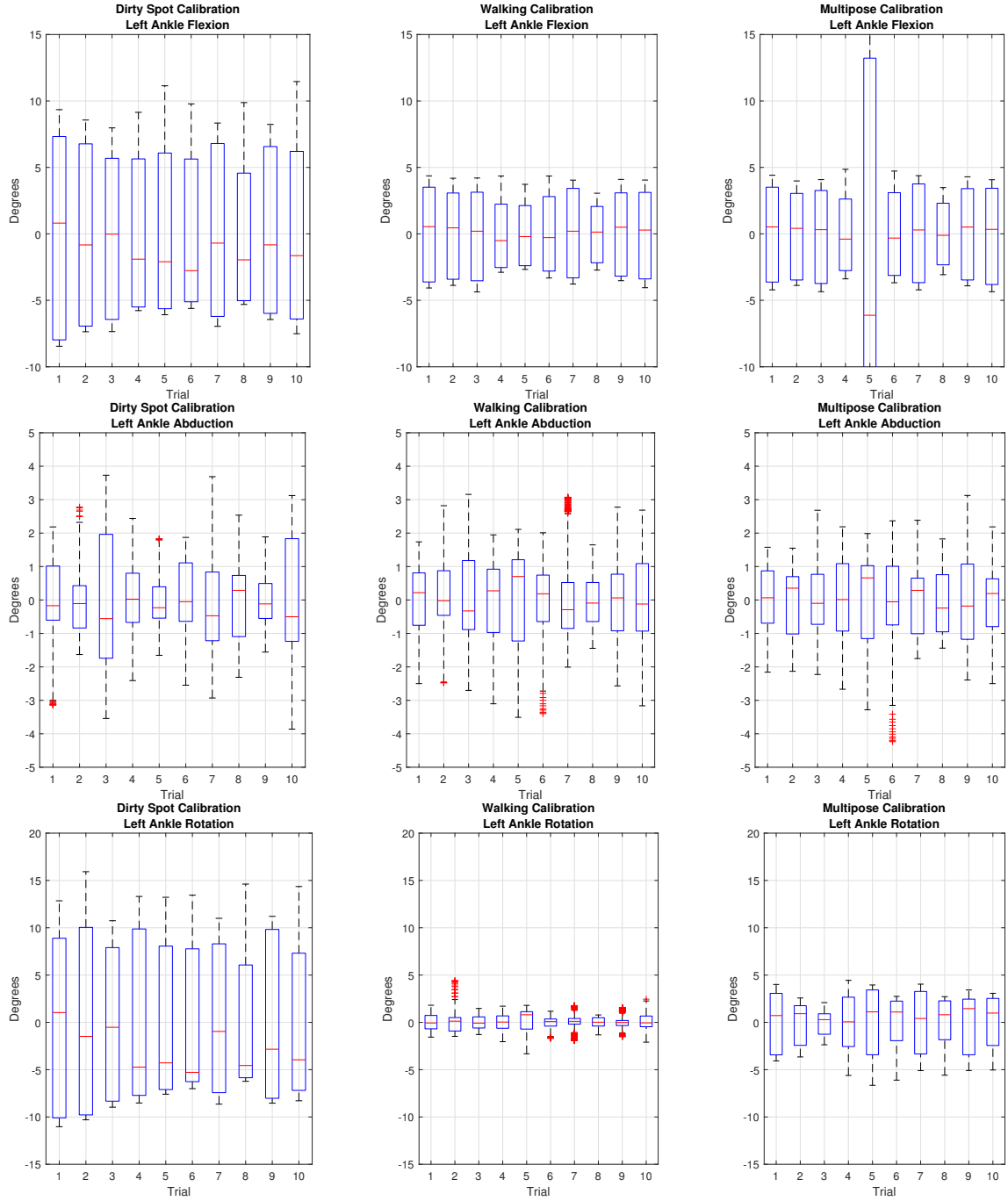


Figure 37: Dirty spot calibration, boxplots left ankle

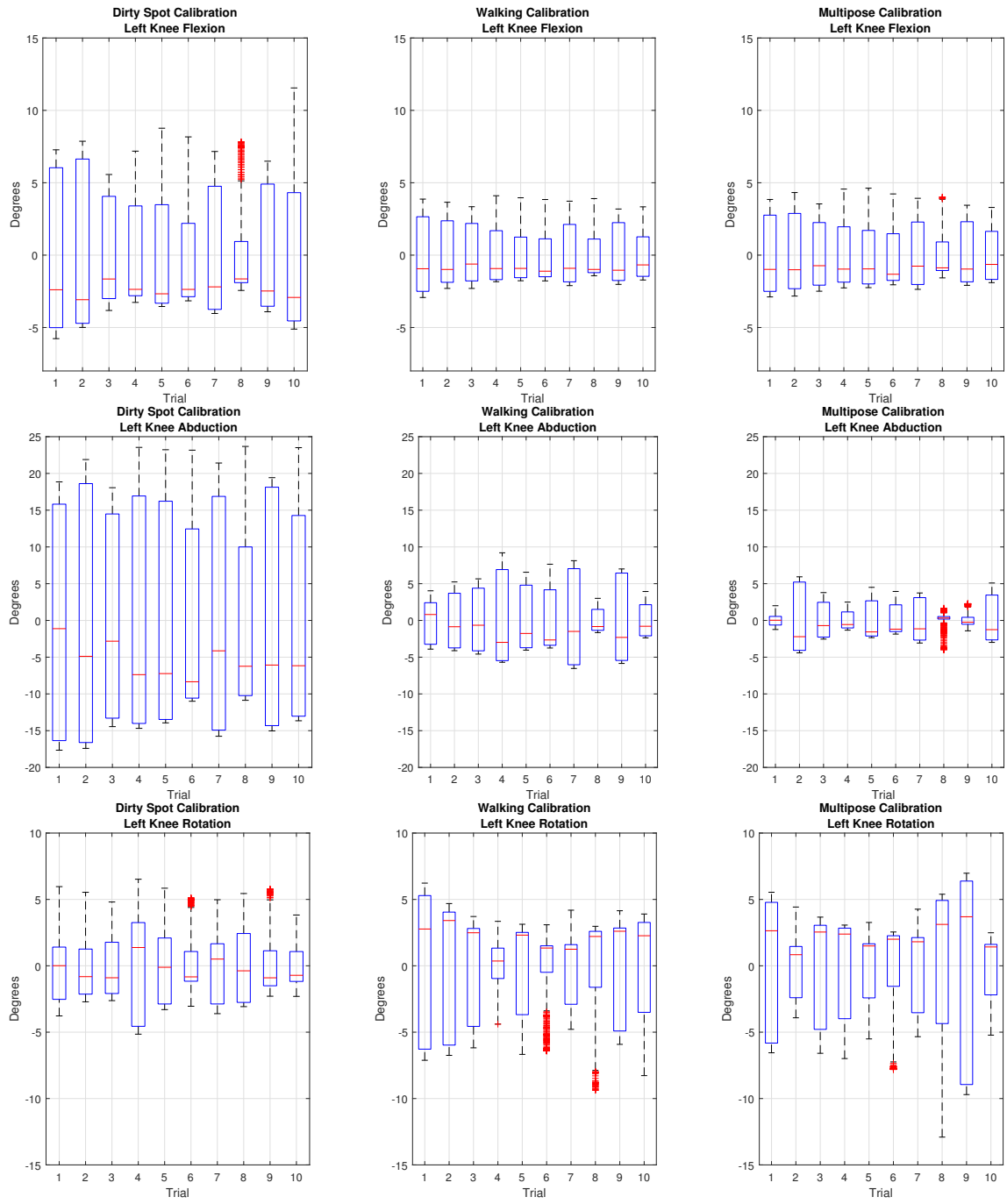


Figure 38: Dirty spot calibration, boxplots left knee

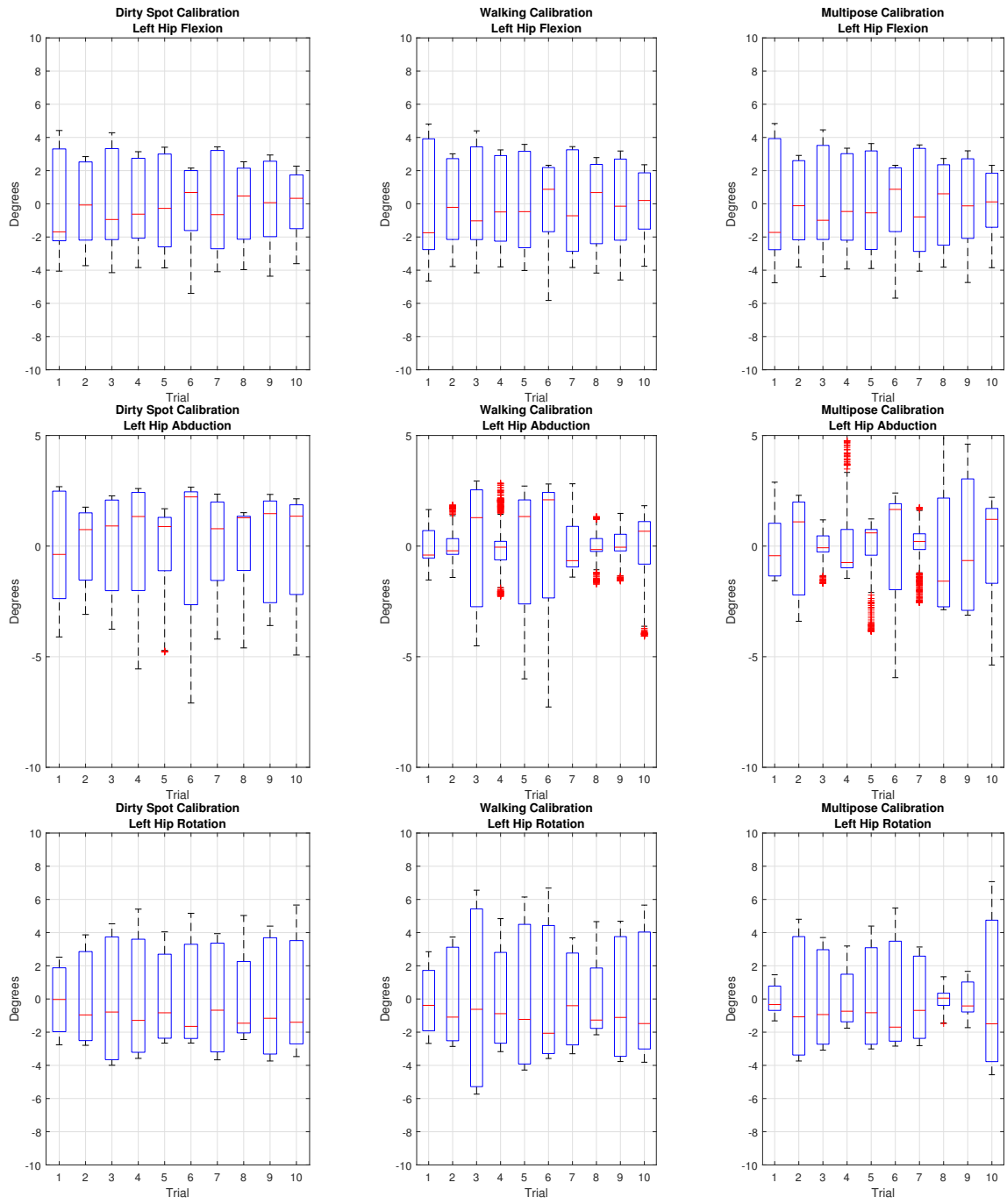


Figure 39: Dirty spot calibration, boxplots left hip

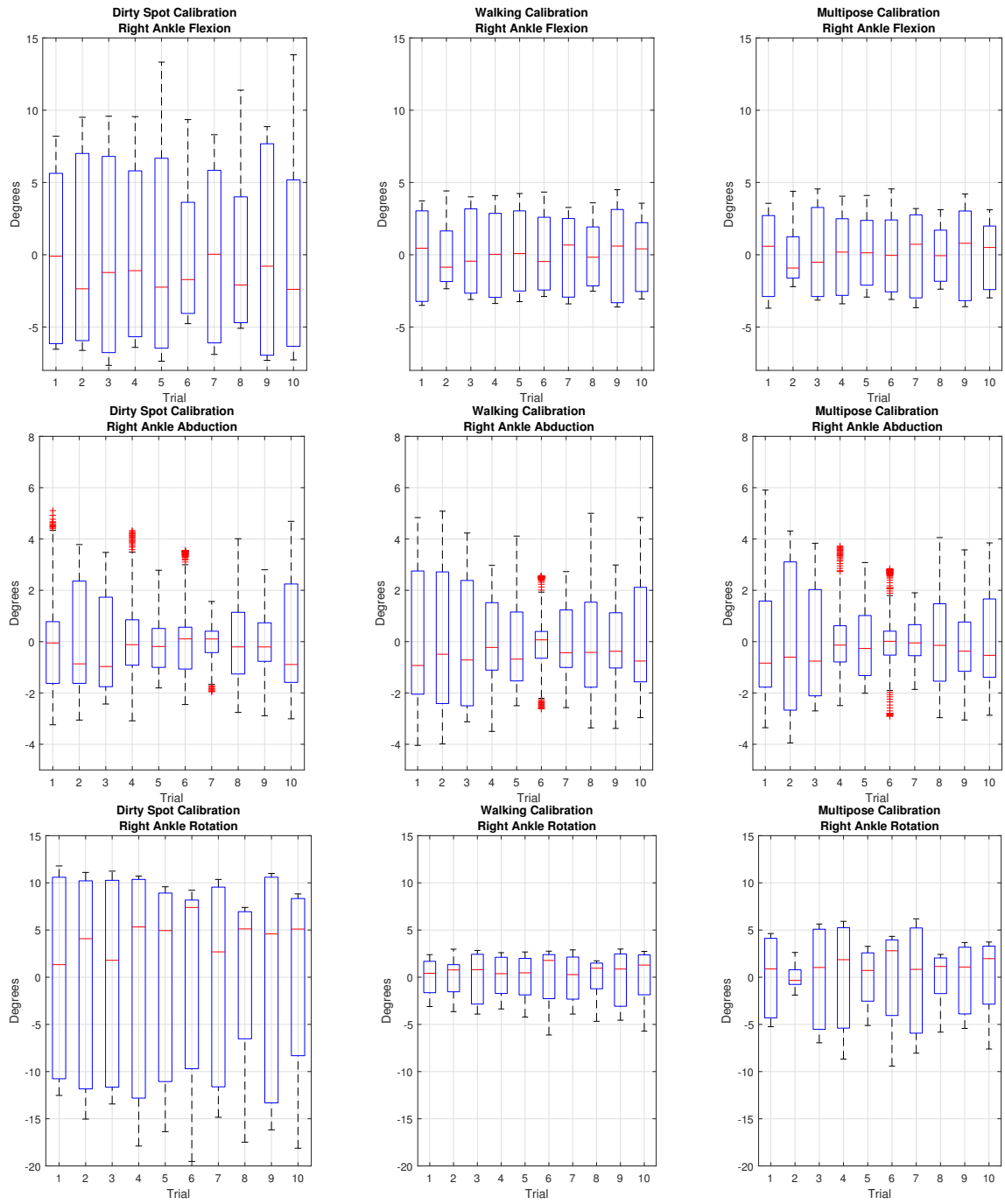


Figure 40: Dirty spot calibration, boxplots right ankle

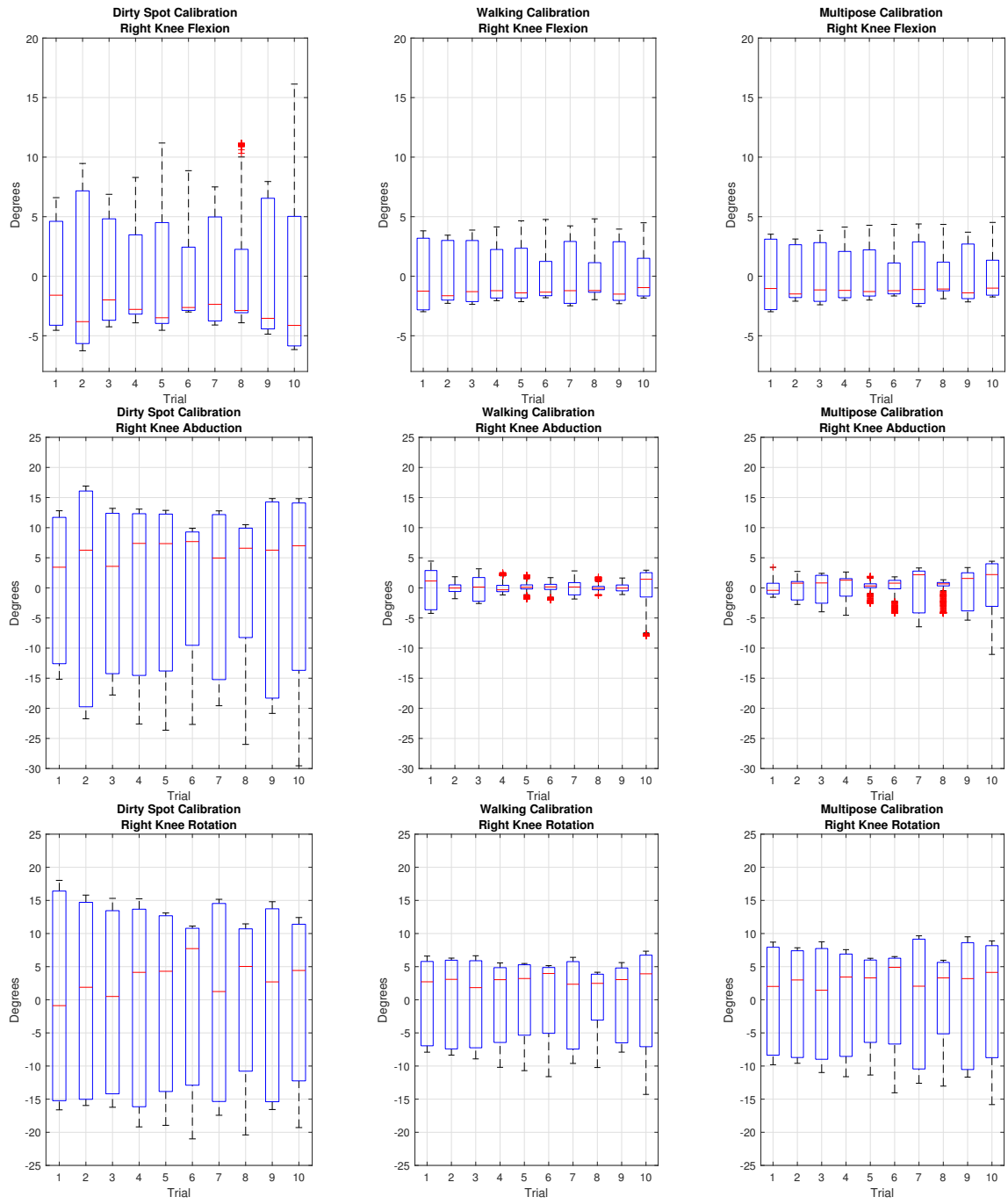


Figure 41: Dirty spot calibration, boxplots right knee

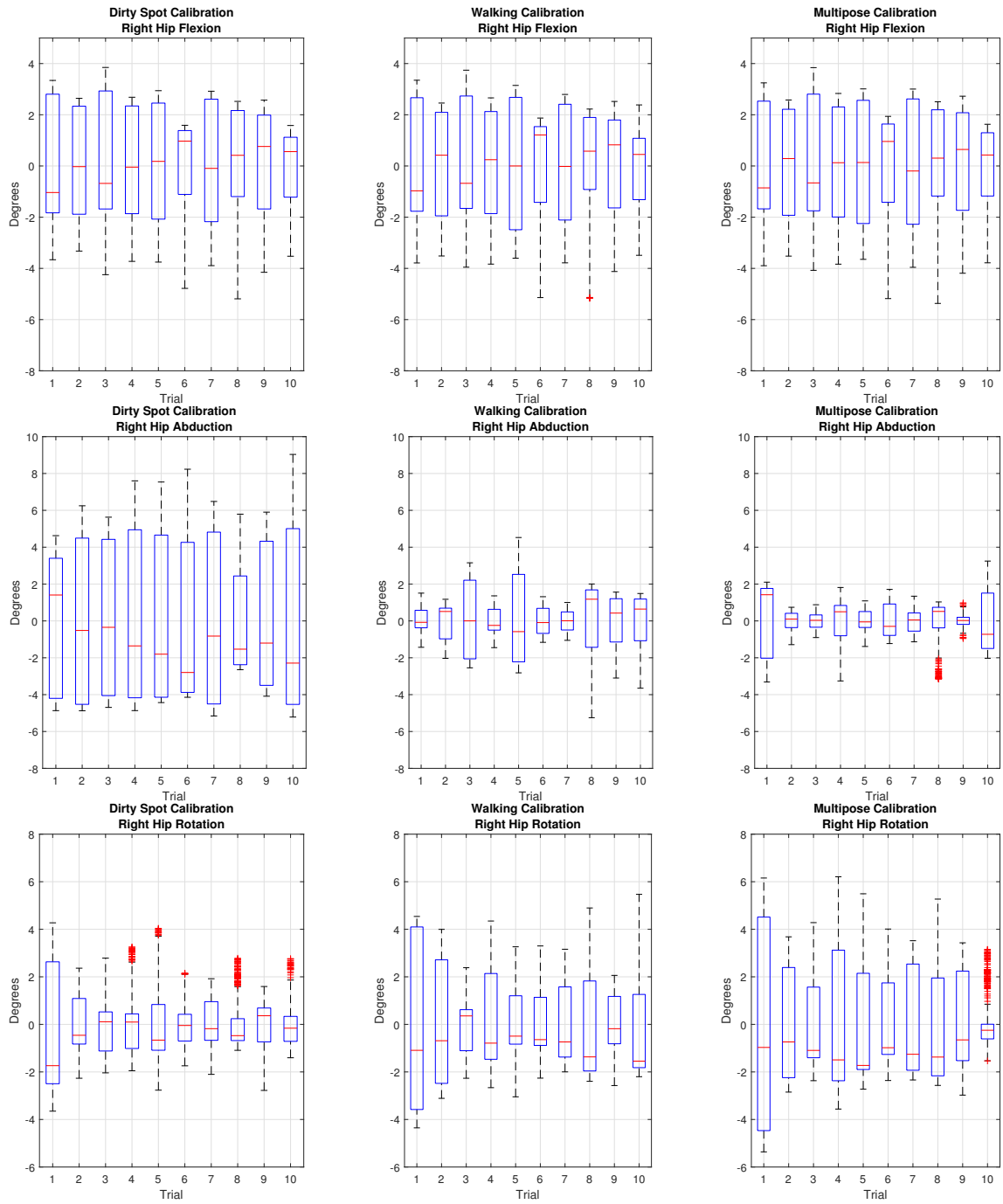


Figure 42: Dirty spot calibration, boxplots right hip

B.2 Clean Spot Calibration

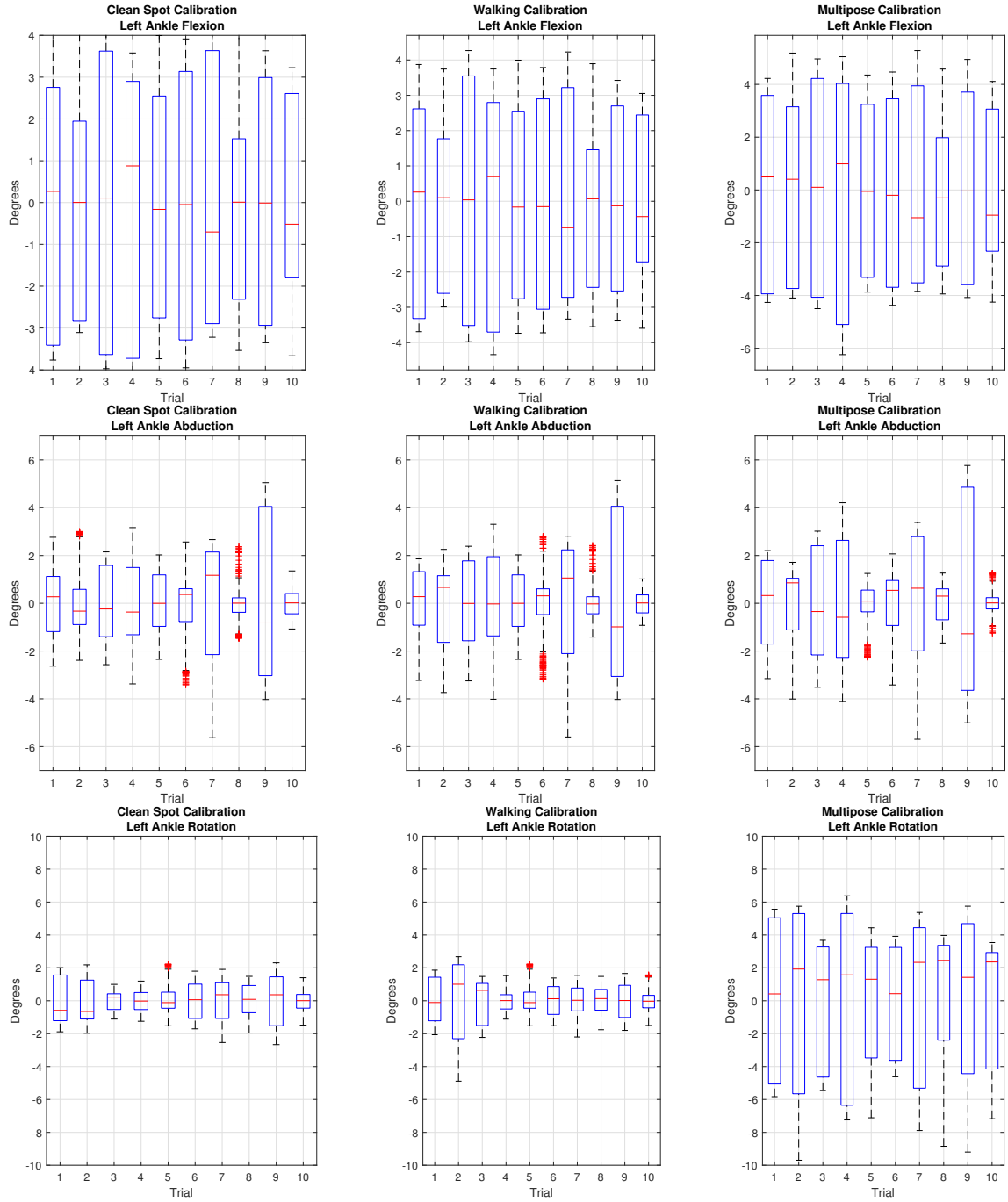


Figure 43: Clean spot calibration, boxplots left ankle

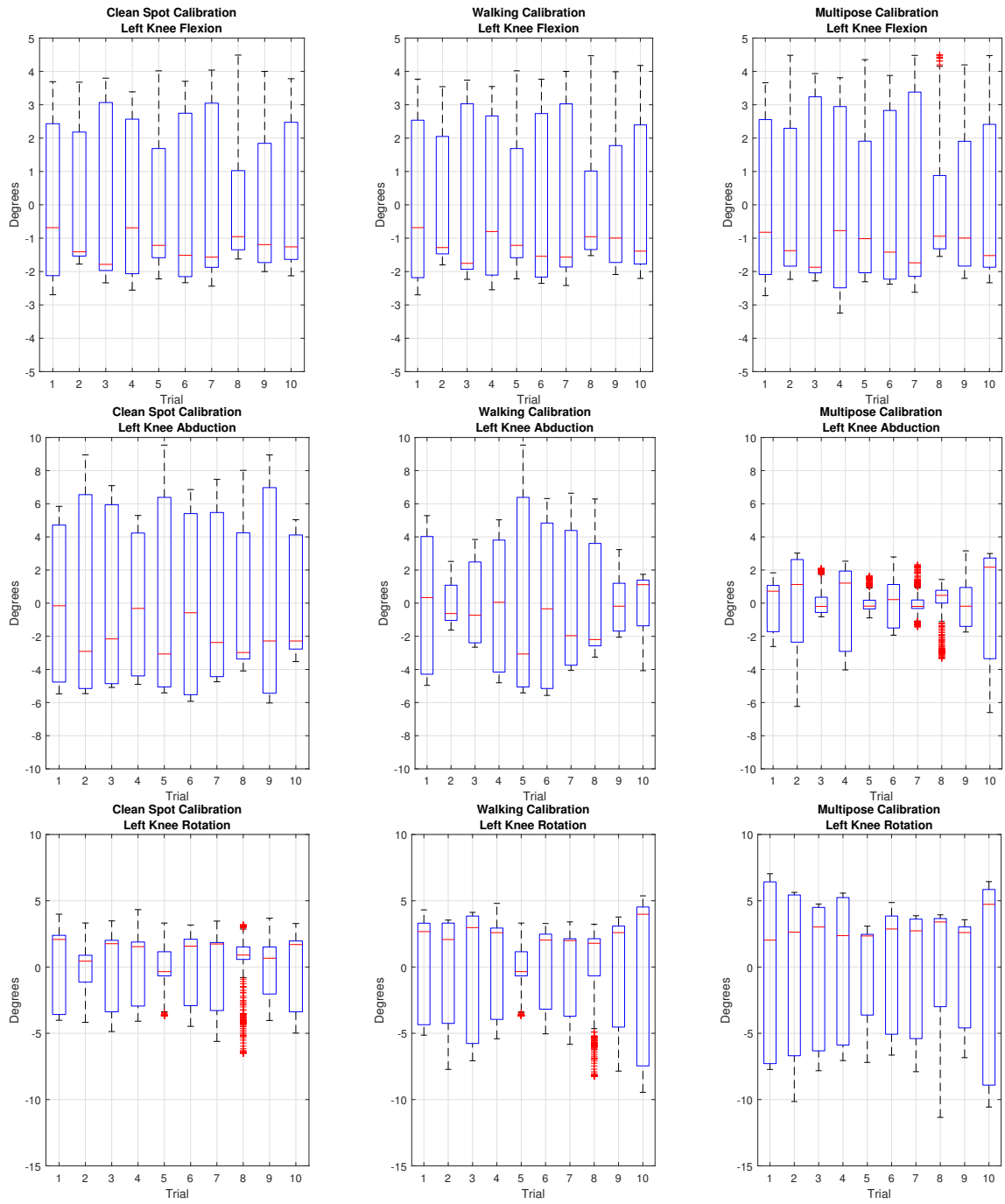


Figure 44: Clean calibration spot, boxplots left knee

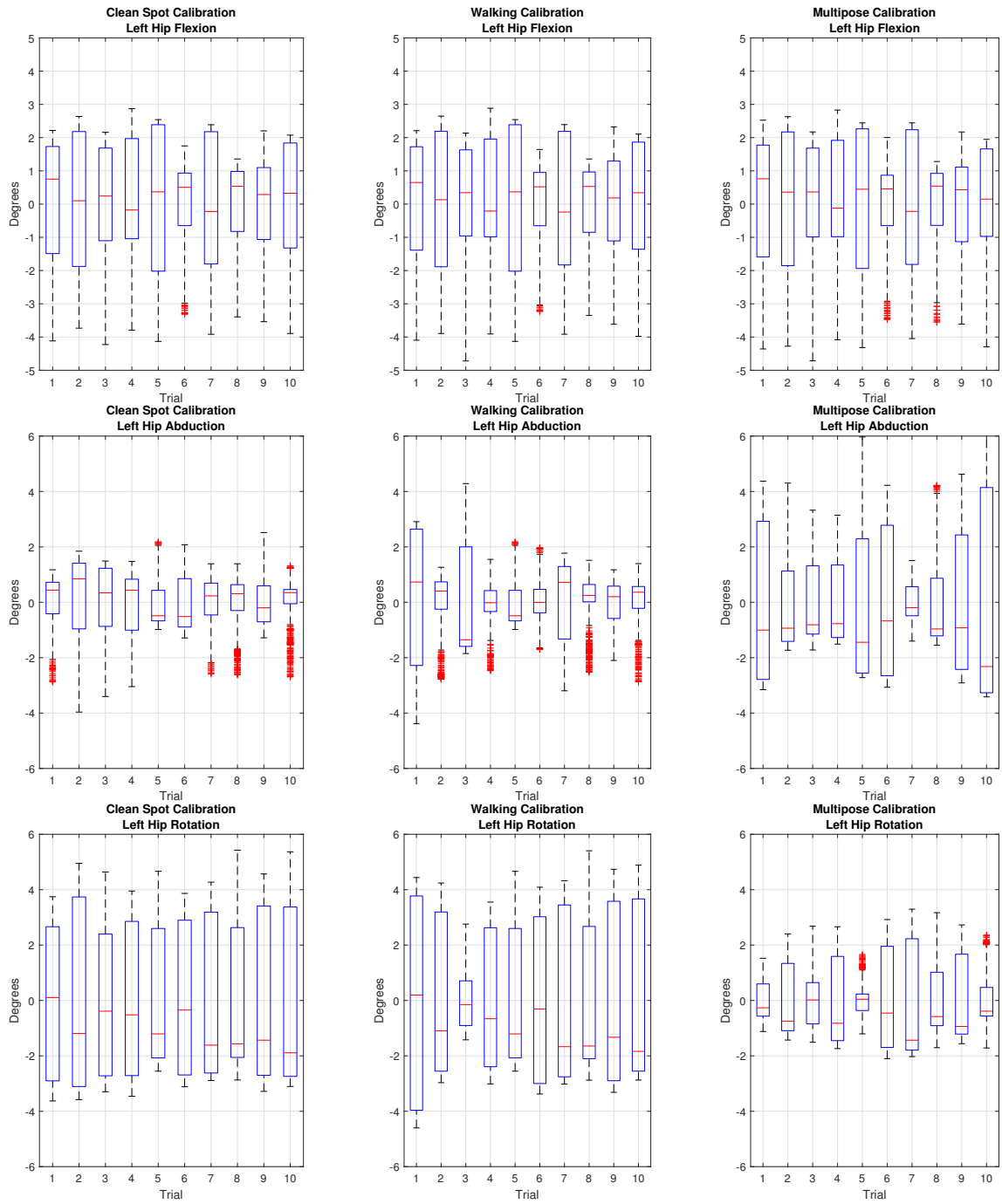


Figure 45: Clean calibration spot, boxplots left hip

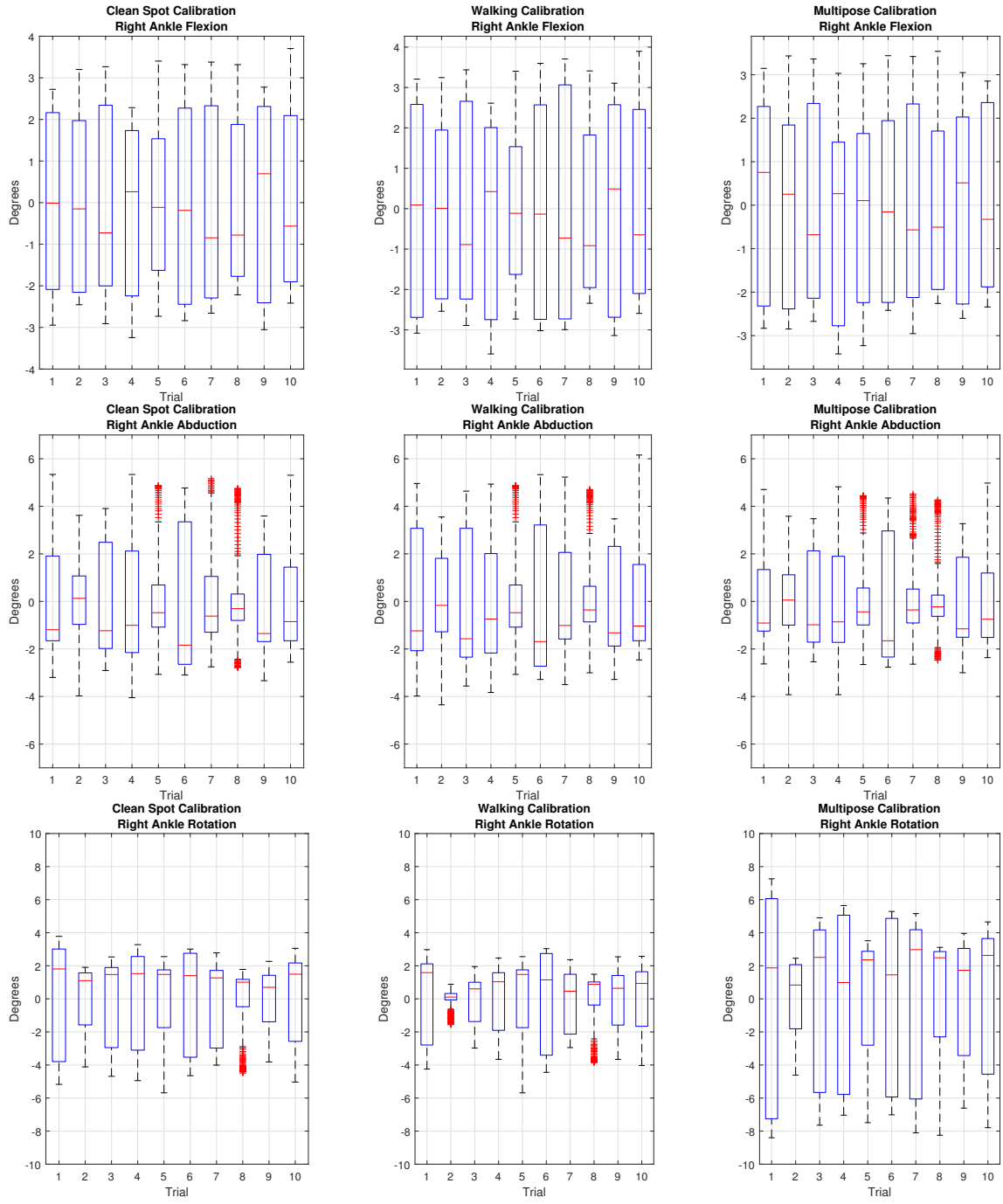


Figure 46: Clean spot calibration, boxplots right ankle

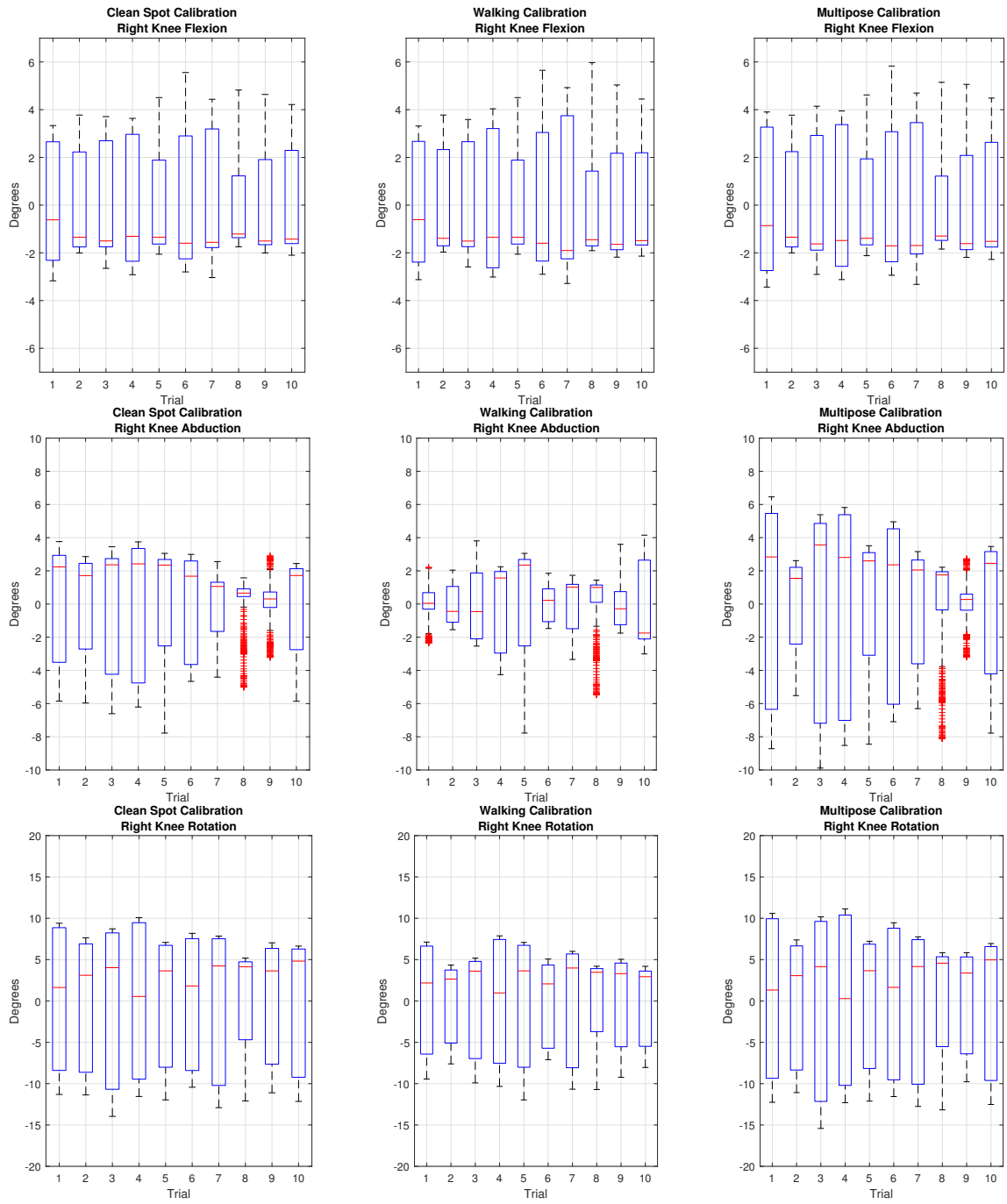


Figure 47: Clean calibration spot, boxplots right knee

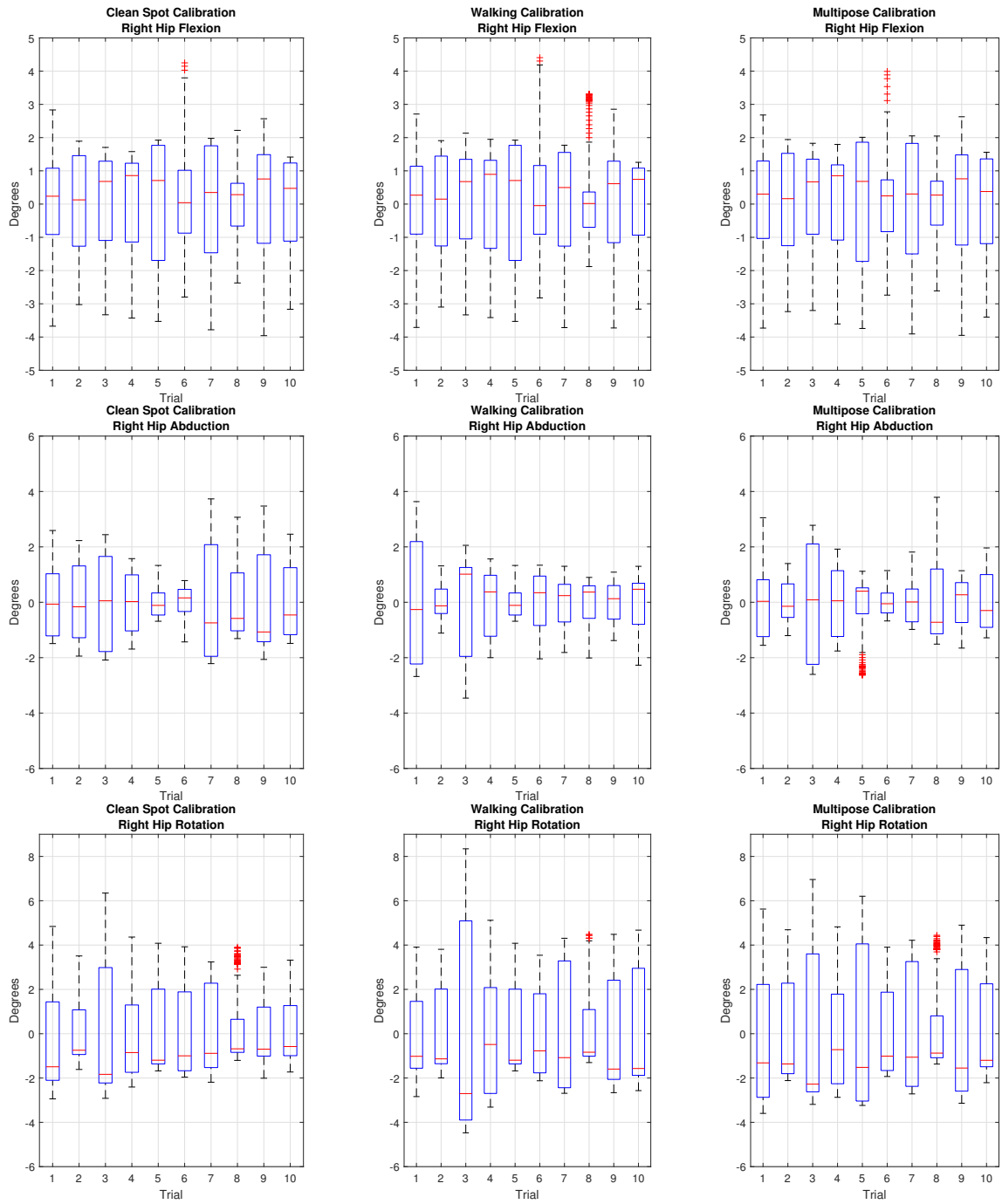


Figure 48: Clean calibration spot, boxplots right hip

C Offset tables

Offsets to Reference, mean Values and Standard deviation. All Values in °

Left Ankle			Right Ankle		
	mean	STD		mean	STD
WC Flexion	-1,56	0,68	WC Flexion	-5,68	0,69
MP Flexion	-3,57	5,06	MP Flexion	-4,70	0,49
Restored Flexion	-5,50	0,88	Restored Flexion	-12,16	2,69
WC Abduction	1,85	3,42	WC Abduction	14,19	4,89
MP Abduction	8,21	2,01	MP Abduction	4,37	3,61
Restored Abduction	6,54	2,21	Restored Abduction	4,53	4,00
WC Inversion	-1,76	2,21	WC Inversion	10,37	2,74
MP Inversion	1,95	2,45	MP Inversion	12,25	3,60
Restored Inversion	-12,55	1,89	Restored Inversion	18,99	3,26
Left Knee			Right Knee		
	mean	STD		mean	STD
WC Flexion	2,31	0,83	WC Flexion	-1,29	1,14
MP Flexion	1,97	0,92	MP Flexion	-1,18	0,98
Restored Flexion	-0,87	1,45	Restored Flexion	-5,81	2,79
WC Abduction	0,10	2,29	WC Abduction	3,61	2,52
MP Abduction	3,07	2,83	MP Abduction	6,85	2,66
Restored Abduction	-14,72	2,25	Restored Abduction	22,44	3,68
WC Rotation	2,84	3,85	WC Rotation	2,27	3,96
MP Rotation	4,65	3,04	MP Rotation	5,82	4,47
Restored Rotation	-1,23	3,18	Restored Rotation	11,96	4,98
Left Hip			Right Hip		
	mean	STD		mean	STD
WC Flexion	-4,43	1,64	WC Flexion	-5,76	1,40
MP Flexion	-4,46	1,59	MP Flexion	-5,49	1,31
Restored Flexion	-4,71	1,52	Restored Flexion	-5,81	1,26
WC Abduction	-4,09	2,17	WC Abduction	-3,92	2,00
MP Abduction	-5,79	3,46	MP Abduction	-3,80	1,97
Restored Abduction	-2,60	1,16	Restored Abduction	-10,03	1,61
WC Rotation	-2,53	4,07	WC Rotation	1,15	5,09
MP Rotation	-4,23	2,09	MP Rotation	5,26	1,84
Restored Rotation	-5,06	1,76	Restored Rotation	6,99	1,80

Table 9: Offsets to Reference, Dirty Spot Calibration Trials

Offsets to Reference, mean Values and Standard deviation. All Values in °

Left Ankle			Right Ankle		
	mean	STD		mean	STD
WC Flexion	-0,210	0,91	WC Flexion	-5,12	0,85
MP Flexion	-2,266	0,82	MP Flexion	-3,69	1,07
Restored Flexion	0,189	0,99	Restored Flexion	-4,66	0,93
WC Abduction	0,243	3,66	WC Abduction	12,70	4,78
MP Abduction	7,077	3,11	MP Abduction	3,19	1,75
Restored Abduction	6,149	3,20	Restored Abduction	2,73	1,88
WC Inversion	2,211	2,14	WC Inversion	13,53	1,87
MP Inversion	7,356	2,76	MP Inversion	16,77	1,91
Restored Inversion	1,656	1,45	Restored Inversion	14,37	1,40
Left Knee			Right Knee		
	mean	STD		mean	STD
WC Flexion	3,00	1,17	WC Flexion	-2,31	0,64
MP Flexion	2,10	0,88	MP Flexion	-2,74	0,42
Restored Flexion	3,00	1,18	Restored Flexion	-2,20	0,44
WC Abduction	1,99	3,13	WC Abduction	4,88	2,97
MP Abduction	7,27	2,43	MP Abduction	9,78	1,39
Restored Abduction	-1,09	1,57	Restored Abduction	8,17	0,81
WC Rotation	5,88	5,09	WC Rotation	3,06	4,72
MP Rotation	10,18	2,68	MP Rotation	6,75	2,26
Restored Rotation	6,49	2,90	Restored Rotation	6,33	2,51
Left Hip			Right Hip		
	mean	STD		mean	STD
WC Flexion	-4,25	1,42	WC Flexion	-6,89	1,60
MP Flexion	-4,34	1,35	MP Flexion	-6,56	1,70
Restored Flexion	-4,35	1,36	Restored Flexion	-6,63	1,67
WC Abduction	-3,54	1,78	WC Abduction	-1,62	1,31
MP Abduction	-7,33	1,18	MP Abduction	-2,67	1,32
Restored Abduction	-3,42	1,05	Restored Abduction	-3,80	1,51
WC Rotation	-2,54	4,64	WC Rotation	3,20	3,88
MP Rotation	-4,95	2,61	MP Rotation	5,80	2,82
Restored Rotation	-6,98	2,55	Restored Rotation	6,81	2,57

Table 10: Offsets to Reference, Clean Spot Calibration Trials